Nitrosation and nitration of diclofenac and structurally related nonsteroidal anti-inflammatory drugs (NSAIDs) in nitrifying activated sludge

Victoria Osorio[1,2,3*], Alberto Cruz-Alcalde[1], Sandra Pérez[1]

[1] ENFOCHEM, IDAEA-CSIC, c/Jordi Girona 18-26, 08034 Barcelona (Spain).

[2] Catalan Institute for Water Research (ICRA), Emili Grahit 101, 17003 Girona, Spain

[3] Department of Chemistry, University of Girona, c/ Maria Aurèlia Capmany, 69, E-17003, Girona (Spain)

*Corresponding author:

Victoria Osorio

Catalan Institute for Water Research (ICRA)

Water Quality Research Group

C/Emili Grahit 101

17003 Girona, Spain

E-mail: vosorio@icra.cat

Phone: +34 972183380

Keywords

Pharmaceuticals, nitrifying microbial community, isotopically labelled ammonia, nitro and nitroso biotransformation products, structural elucidation, high-resolution mass spectrometry

ABSTRACT

Diclofenac (DCF) is a highly consumed non-steroidal anti-inflammatory drug that is excreted partially metabolized and is poorly removed during wastewater treatment. Previous findings demonstrated that DCF in wastewater treatment plants (WWTP) is partially removed to nitro/nitroso compounds. The reactive nitrogen species, that are microbially produced during nitrification in the activated sludge of WWTP, were suspected to be involved in the transformation of DCF. Therefore, here, we investigated the molecular features governing such biotransformation and the role played by nitrifying bacteria by biodegradation experiments at lab scale in enriched nitrifying sludge bioreactors spiked with DCF and other structurally related non-steroidal anti-inflammatory drugs (NSAIDs). We provided evidence of the incorporation of NO/NO_2 groups into DCF originated from ammonia by isotopically labelled biodegradation experiments. Nitroso and nitro-derivatives were tentatively identified for all NSAIDs studied and biotransformation mechanisms were proposed. Our findings from biodegradation experiments performed under different incubation conditions suggested that biotransformation of DCF and its related NSAIDs might not only be microbially mediated by ammonia oxidizing bacteria, but other nitrifiers co-occurring in the activated sludge as ammonia oxidizing archaea and nitrite oxidizing bacteria. Follow-up studies should be conducted to disentangle such complex behaviour in order to improve removal of these contaminants in WWTPs.

1. Introduction

Due to demographic, social and economic factors, the production and use of pharmaceuticals in industrialized societies has increased to considerable levels [1]. For instance, non-steroidal anti-inflammatory drugs (NSAIDs) are produced annually worldwide in the range of kilotons [2]. NSAIDs are a large group of chemically heterogeneous drugs that are used primarily to treat inflammation, mild to moderate pain, and fever. After their use in human medicine, 1-90% of the parent drug passes through the human body completely unchanged [3]. They may then reach surface waters via hospital and municipal sewage [4]. The impact of this kind of pollution in surface water is usually attenuated at the wastewater treatment plant (WWTP) discharge point by dilution of the effluents, at varying ratios, with the receiving water bodies. However, under dry weather conditions or intensive human activity these may significantly reduce their water flow or volume, resulting in lower dilution ratios and a higher concentration of contaminants. Cases in point of this situation are intermittent rivers [5]. Among NSAIDs, diclofenac (DCF), with high consumption rates, has been frequently detected at high levels in influent (500-7500 ngL^{-1}) and effluent (200-1400 ngL^{-1}) wastewater (WW) and sludge (70 $ngKg^{-1}$) samples from WWTPs [6,7]. In full-scale WWTP relying on conventional activated sludge treatment, removal efficiencies for DCF are widely varying, [7-80] % [8], rendering it difficult to identify common patterns in its biotransformation.

Being excreted partially metabolized, DCF together with its metabolites, may undergo further transformation along their fate in the technosphere and the environment. Little is known about the biotransformation pathways of DCF in complex microbial communities like those encountered in the aeration tank of the conventional activated sludge treatment. Nitrification in the activated sludge is an essential step for the removal of ammoniacal nitrogen in WWTPs. In many WWTPs, this first stage of the nitrogen removal process is microbially driven by autotrophic nitrifiers such as Ammonia-oxidizing bacteria (AOBs), transforming ammonia to nitrite (NO_2^-); and Nitrite-oxidizing bacteria (NOBs), converting NO_2^- to nitrate (NO_3^-) [9]. However, ammonia-oxidizing archaea (AOA), transforming NH_3 to NO_2^-; heterothropic nitrifiers capable to oxidize NH_3 as well, and complete ammonia oxidizers (comammox), converting NH_3 to NO_3^- on their own, may also be present in the activated sludge having a role in the nitrification process [10–12]. During nitrification process in the conventional activated sludge, reactive nitrogen species such as nitric oxide (NO•) are generated, which are suspected to be involved in the formation of Transformation Products (TPs) containing nitro or nitroso groups such as nitro-acetaminophen [13], 5-nitro-DCF (NO_2-DCF or TPDCF340) or N-nitroso-DCF (NO-DCF or TPDCF324) identified in our previous work [14]. We anticipated that NO• was responsible for the N-nitrosation and C-nitration of DCF [15]. Other works have also suggested such reactions to occur for secondary amines as DCF and Mefenamic Acid under nitrifying activated sludge treatment [13,16–18].

As a consequence of the recalcitrant behaviour during the conventional treatment in WWTPs, DCF has been detected elsewhere in fresh-water, marine and terrestrial environmental compartments and even in biota at the low to high trace levels [7,19–23]. Owing to its pseudo-persistence in the aquatic environment and ecotoxicological impact, DCF was included in the EU Commission watch list of organic pollutants in SW [24]. However, DCF is no longer considered among the top priority contaminants of emerging concern in the environment [25]. The associated risks to DCF spread in the environment might be misinterpreted due to the gap of knowledge about the potential ecotoxicological effects of unknown derivatives of this drug. The bioactivity exerted by TPs might be more relevant than the parent drug itself, contributing to synergistic, addition or antagonistic toxic effects in mixtures of them [26,27]. Indeed, we evidenced that 5-nitro-DCF is more toxic to *Vibrio Fischeri* than DCF and N-nitroso-DCF showed synergistic effects in mixtures with other contaminants of emerging concern at environmentally relevant concentrations [28]. We demonstrated the release of TPDCF324 and TPDCF340 into SW (5-15 ngL^{-1}) via WW effluents (4-105 ngL^{-1}) from Catalan WWTPs, which also suggested the potential in-sewage transformation (4-8 ngL^{-1} in WW influent) of DCF into these concerning TPs [15,29]. Given these facts, the formation and dissemination of Nitroso- and Nitro-derivatives of DCF in the technosphere and the environment, is a matter of relevant concern that needs to be further investigated.

The two main aspects of our research were to understand the molecular features that govern the formation of nitroso- and nitro- TPs from DCF and the role played by nitrifying bacteria in this process. Thus, biodegradation experiments were conducted under controlled laboratory settings in enriched nitrifying activated sludge bioreactors spiked with DCF and five structurally related compounds, namely: 2-anilinophenylacetic acid (APAA), meclofenamic acid (MCF), flufenamic acid (FFN), tolfenamic acid (TFM), and mefenamic acid (MFN) (Figure 1). This selection of compounds enabled to compare the effect of the class of the acidic moiety (phenylacetic acid in APAA and DCF vs. benzoic acid in FFN; MCF, MFN, and TFM) and that of the substitution pattern of the aniline ring (substituent-free in APAA vs. different combinations of methylation and halogenation in DCF, FFN, MCF; MFN, and TFM). In a first set of experiments, we sought to generate evidence that the NO/NO_2 groups incorporated into the substrates originated from ammonia. To this end, DCF-spiked bioreactors were repeatedly supplemented with ^{15}N-labeled ammonia during the incubations to induce the formation of the respective TPs exhibiting the diagnostic isotope-related mass shifts. Afterwards, samples from different bioreactors individually spiked with DCF and APAA were analysed by high-resolution mass spectrometry (HR-MS) to confirm the identity of the expected TPs and to assess the extent and rate of their formation. Lastly, we tested the hypothesis of ammonia oxidizers to play a crucial role in the conversion of DCF and the other analogues to its NO/NO_2 derivatives by performing incubations in the presence of allylthiourea as a selective inhibitor of AOB, which we believed to trigger the reaction cascade eventually leading to formation of these species.

2. Materials and methods

2.1. Chemicals and standards

Diclofenac was purchased from Sigma-Aldrich (Steinheim, Germany), while the following were obtained from Toronto Research Chemicals (Toronto, Canada): 2-anilinophenylacetic acid (APAA), mefenamic acid (MFN), tolfenamic acid (TFM), meclofenamic acid (MCF) and flufenamic acid (FFN). Allylthiourea (ATU), sodium azide (SA) and ammonium acetate were provided by Sigma-Aldrich (Steinheim, Germany). Formic acid (98%-100%), acetic acid (98-100%), ammoniumhydroxide (36%) and $^{15}NH_4$ ammonium hydroxide (36%) were purchased from Merck (Darmstadt, Germany). All solvents (methanol, acetonitrile and water) were purchased from Fisher Scientific (Geel, Belgium). Calibration of the Q-Exactive Orbitrap-MS was performed with ESI negative and positive ion calibration solutions from Thermo Scientific (Dresden, Germany).

2.2. Biodegradation experiments

2 L amber glass bottles were loaded with one liter of mixed liquor freshly collected from the nitrification tank of the WWTP of Rubi (Catalonia, Spain) and spiked with every individual NSAID at 10 mgL^{-1}. The pH of the mixed liquor in the batch-reactors was maintained at 7.4±0.3, while the ambient temperature was 20-22 ºC. Bubbling of air through Teflon tubing into the test medium provided continuous aeration of the system and ensured suspension of the sludge particulate matter (5 gL^{-1}) to avoid anoxic and anaerobic respiration. To ensure the activity of the ammonium oxidizers, all reactors were supplemented with ammonia on-a-daily basis. To prevent evaporation and photolytic degradation, glass reactors covered on top with aluminium foil and parafilm were used.

Transformation of DCF in the presence of the Isotope labelled ammonia. Two batch-reactors were spiked with DCF at 10 mgL-1 and supplemented with NH_4^+ while $^{15}NH_4^+$ was added to the other one. Samples were collected for 20 days.

Transformation of DCF and its non-chlorinated analog (APAA). Batch-reactors individually spiked with DCF and APAA were monitored during 20 days of biodegradation.

Transformation of DCF and four related fenamates. Batch-reactors individually spiked with the five NSAIDs: DCF, MCF, FLUF, TFM, and MFN at 10 mg L/1 for 63 days. In parallel, two reactors were run at the same test concentration only with DCF and one of which was treated with the AOB/specific inhibitor ATU (5 mgL^{-1}) whereas the other was not supplemented with ammonia to induce starvation of AOBs.

Biologically inactive control batch-reactor spiked with a mixture of compounds at 10 mgL^{-1} were run in parallel in all experiments through addition of SA (10 mgL^{-1}) to account for any abiotic removal mechanisms. The concentration (mgL^{-1}) of ammonia, nitrates and nitrites, as well as pH,

was qualitative controlled in all reactors on a daily basis using test strips in order to ensure optimal nitrification conditions.

At defined time points 2 ml aliquots were withdrawn from each batch reactor. One hundred microliters of methanol were added and the samples were centrifuged at 4000rpm for 10 min at 10 ◦C. The supernatant was stored at −20◦C until instrumental analysis.

2.3. Structural elucidation of TPs

To elucidate the structures of the transformation products of DCF, MCF, FLUF, TFM, and MFN in the bioreactor an ultra-performance liquid chromatography (UPLC)-/(-)-heated electrospray ionization (HESI)-Q Exactive Orbitrap-MS working in negative ionization mode was used. Chromatographic separation was achieved on a Waters Acquity BEH C18 column (100 × 2.1 mm, 1.7-µm particle size) equipped with pre-column (50 × 2.1 mm) of the same packing material. The mobile phases were (A) 10 mM aqueous ammonium acetate/ acetic acid (pH 5.8) and (B) acetonitrile. The elution gradient started with 10 % B, increase to 95 % in 11 min and return to initial conditions after 2 min. The column was re-equilibrated for 1.5 min. Flow rate was 0.3 ml min^{-1} and the sample injection volume was set at 10 µl. Data acquisition was carried out in full-scan mode scan range of 100-800 m/z and data dependant MS^2 in discovery mode with resolution settings of 70.000 and 35.000, respectively. The ESI source was operated at a spray voltage of 4.0 kV and a capillary temperature of 350 ºC. All MS data acquisition and processing were done using the Xcalibur V2.2.

Accurate mass measurements of DCF, APAA as well as their biotransformation products formed in the batch-reactors were carried out in full-scan and product ion scan mode using a Micromass QqToF-system interfaced with a Waters ACQUITY UPLC system (Micromass, Manchester, UK) on a Waters ACQUITY BEH C18 column (50 × 2.1 mm, 1.7 µm particle size) equipped with precolumn (5 × 2.1 mm) of the same packing material. The mobile phases were (A) 10 mM aqueous ammonium acetate/acetic acid (pH 5.8) and (B) acetonitrile [14]

2.4. Bacterial cell viability on activated sludge

To evaluate the cell viability in the different batch/reactors, live and dead cells at the end of the biodegradation in the experiment of transformation of DCF and their halogenated structurally related fenamates. Live and dead cell ratios were investigated with epifluorescence microscopy. Live and dead bacteria, identified as intact cells and membrane compromised cells, respectively, were stained using the LIVE/DEAD® Bacteria Viability Kit L7012 (BackLight™, Molecular Probes, Invitrogen L7012). The activated sludge of every bioreactor was filtered through 0.2 µm black polycarbonate filters (Nuclepore, Whatman). Filters were then dried, placed on a slide with mounting oil (Molecular Probes) and counted by epifluorescence microscopy (Nikon E600, 1000 in

immersion oil). Green and red (live and dead, respectively) bacteria cells were counted in 20 random fields per filter.

3. RESULTS AND DISCUSSION

3.1 Transformation of DCF in the presence of the Isotope labelled ammonia

Based on our previous findings [13,15,18], it was hypothesized that the formation of nitrosated/nitrated TPs involved ammonia oxidation by specific nitrifying microorganisms. To test this hypothesis, their maintenance and growth was ensured by daily addition of $^{15}NH_4^+$. By adding $^{15}NH_4^+$, the incorporation of the stable isotope N, would result in a mass shift of their respective molecular ions by 1 m/z unit. With the presence of $^{15}NH_4$ in the reactors, the formation of ^{15}NO-DCF (TPDCF324) and $^{15}NO_2$-DCF (TPDCF340) was expected. Accurate mass spectra acquired for TPDCF324 and TPDCF340 observed in bioreactors treated with $^{15}NH_4^+$ and $^{14}N\text{-}H_4^+$ were compared (Figures 2 a-d).

A mass shift of +1 Da was expected to be observed in the molecular mass of TPDCF324, which would correspond to the nitroso- derivative of DCF after inclusion of ^{15}NO group into the molecule. As it can be noticed in Figure 2b, the additional signal corresponding to the isotope labeled ^{15}NO-DCF (TPDCF324) was identified in the HRMS spectra, compared to the non-isotope-labelled molecule NO-DCF (TPDCF324) (Figure 2a) where no additional peak corresponding to a mass shift of +1 Da was detected. The incorporation of ^{15}NO group into DCF was in line with the radical loss of -COO^{15}NO, corresponding to a mass shift of 75 Da (figure 2b), while the mass shift of 74 Da (figure 2a) was assigned to the fragmentation of -COONO from molecular ion m/z 323. Regarding TPDCF340, a mass shift of +1 Da also expected due to incorporation of $^{15}NO_2$ group into the DCF molecule was observed (Figure 2c). MS spectra observed for NO_2-DCF (TPDCF340) (Figure 2c) and isotope-labeled $^{15}NO_2$-DCF (TPDCF340) (Figure 2d), allowed confirming position of NO_2 group in the molecule.

As proposed previously for nitro-acetaminophen [13] and for nitroso and nitro-TPs of DCF [28], reactive nitrogen species that are produced during the nitrification process by nitrifying bacteria. In particular, NO• is a highly reactive species that is produced by both nitrification and denitrification processes. Under aerobic conditions, NO• easily reacts with molecular oxygen under anaerobic conditions resulting in the formation of dinitrogen trioxide (N_2O_3), or, with the superoxide radical anion ($O_2^{\bullet -}$), producing peroxynitrite ($ONOO^-$) [30]. N_2O_3 and $ONOO^-$ are even more reactive species that can be involved in nitrosation reactions with secondary amines, such as DCF, to produce N-nitroso TPs or C-nitro derivatives [18,28]. They can also react with phenols, giving rise to formation of C-nitroso derivatives [31]. Moreover, reactive nitrogen species are also be involved in N-nitrosation and C-nitration of primary amines such as sulfamethoxazole [17,32,33].

HRMS spectra observed for ^{15}N-nitroso (Figure 2b) and ^{15}N-nitro DCF (Figure 2d) TPs evidenced the respective incorporation of ^{15}NO and $^{15}NO_2$ groups, which could only be derived from oxidation of $^{15}NH_4$ added to the bioreactors. Hence, we rationalize that the stable isotope labelled N in the TPs would provide strong support for their transformation. Since we did not identify such transformation in batch reactors performed under abiotic conditions, we accounted nitrifiers to be responsible for the transformation of DCF into TPDCF324 and TPDCF340. However, further isotope labelled biodegradation experiments should be performed monitoring the evolution of $^{15}NH_4$ to nitrite and nitrate species during nitrification process. This assessment would provide further insight on the role of triggered RNS in nitrosation and nitration mechanisms of DCF.

3.2 Transformation of DCF and its non-chlorinated analogue

According to biodegradation profiles obtained from the second transformation experiment (see Figure A-1), DCF seemed to be recalcitrant, as previously reported [14,34]. Since the biotransformation rates were low in all reactors, it could be related to properties of the compound rather than total organic carbon content in the microcosms [35]. Therefore, it was hypothesized that the two chlorine atoms present in DCF structure hindered the degradation with reactive nitrogen species. To evaluate the effects of the Cl atoms which are relatively large electron withdrawing substituents the reactivity of the non-chlorinated analog, APAA, was assessed. The formation of the nitroso-derivative of APAA was confirmed, no nitrated-TP was detected (Figure 2f). The fragment ion at m/z 181.0936 was formed by concurrent loss of CO_2 and NO•. As observed previously for TPDCF324 [29], such fragmentation pattern suggested that the introduction of a nitroso group in APAA occurred by N-nitrosation.

APAA disappeared in the bioreactor faster than DCF (see Figure A-2 for APAA and Figure A-1 for DCF) with 50% of the initial amount of APAA remaining after one day. This went along with the formation of its nitrosated derivative (Figure A-2). On the other hand, concentrations of DCF remained almost unchanged during the course of the experiment and the formation of TPDCF340 and TPDCF324 was not observed until day 4 and 5, respectively (Figure A-1). DCF stability in in line with it poor removal efficiencies in WWTPs operating with conventional treatment [7,8]. The faster disappearance of APAA compared to DCF, could be attributed to steric hindrance caused by the chlorine atoms which would reduce its reactivity towards NO•. At the same time the Cl atoms exert electron withdrawing effect on the ring which likely renders the NH- less attractive for the attack by the electrophilic NO•.

Therefore, from this experiment, we argued that the low biodegradability of DCF and transformation into TPDCF324 and TPDCF340 could be due to the combination of hindrance effects and poor bacterial diversity, which were strongly affected by the short-term duration of the biodegradation experiments. Owing to these reasons we aimed to perform further long-term biodegradation experiments of at least 60 days in order to compare biodegradability of DCF, as

well as relative abundances of its nitro and nitroso-TPs. Moreover, despite APAA degraded faster, a recovery of the compound was observed from the seventh day of treatment, while TPAPAA256 started to decrease from day 4 (Figure A-2). Such behaviour might be due to the reversible transformation of TPAPAA256 back to its parent compound. The enzymatic hydrolysis of the glucuronide of DCF, a metabolite excreted after consumption together with DCF and detected in WWTPs, was conjectured to occur in-sewage [37]. The transformation of DCF and sulfamethoxazole nitro-TPs back to their parent compound observed under denitrifying conditions was also hypothesized to occur during conventional treatment [32,38]. These observations highlighted the need to conduct further investigations on the underlying biotransformation mechanisms of DCF and other related structures in the activated sludge.

3.3 Transformation of DCF and four related fenamates

3.3.1 Identification and structural elucidation of TPs

Fenamates were added to the reactors in order to evaluate the presence of nitro and nitroso compounds. Figure 3 shows chromatographic retention times for parent compounds and identified TPs and Total Ion Chromatograms and Extracted Ion Chromatograms are shown in Figure A-3. Table 1 summarizes the retention time, elemental composition and exact mass of the 17 TPs tentatively identified in bioreactor extracts analysed. A single isomer of the nitroso TPs was identified for all NSAIDs, namely TPDCF324, TPMCF324, TPFFN310, TPTFM290 and TPMFN270. On the other hand, up to 3 isomers (i.e., species with same fragmentation patterns and corresponding to the same m/z value) were identified as derivatives of the incorporation of an NO_2 into the parent drug, namely, TPDCF340, TPMCF340, TPFFN326, TPTFM306 and TPMFN286. Full scan and MS^n experiments were conducted for the suspect screening and structural elucidation of TPs on aliquots collected daily from the bioreactors. Figures A.3-A.7 show MS and MS^2 spectra acquired for parent compounds in standard solutions and TPs as well as the proposed structures. Table A-1 provides elemental composition, exact mass as well as mass error and double bond equivalent (DBE). The (-)-ESI-MS^2 spectra of parent compounds and potential TPs were compared to elucidate similarities in fragmentation patterns. TPs could be identified by the assignment of elemental formulae based on exact mass, and the interpretation of characteristic product ion spectra allowed to identify the most likely sites of structural modifications in these TPs. A detailed description of fragmentation pathways observed for parent drugs and the diverse derivatives identified is provided in SM.

The NO group present in TPDCF324, TPMCF324, TPFFN310, TPTFM290 and TPMFN270 (Figures A.3-A7 and Table A-1) showed low stability. The elimination of NO, as a radical (NO•) was the common initiator of the fragmentation pathways described for these TPs. Besides, subsequent fragmentation followed the same pattern as parent drugs in all cases. Regarding TPDCF340,

TPMCF340, TPFFN326, TPTFM306, TPMFN286 and their respective isomers, their MS^2 spectra confirmed that the carboxylic acid moiety was not altered during biotransformation of the parent compounds, the initial loss of CO_2 was observed in all cases. Following the fragmentation of all TPs proceeded with the elimination of H_2O, HNO (or NO•) and HX. Overall, the NO_2 group present in these TPs exhibited higher stability in the molecule under (-)-ESI ionization conditions compared to that displayed by the NO group present in TPDCF324, TPMCF324, TPFFN310, TPTFM290 and TPMFN270. Relative isotope abundances provided additional confirmation of those TPs bearing chlorine atoms from DCF, MCF and TFM. The selected NSAIDs were tentatively proposed to transform to nitro and nitroso compounds (Table 1) in a similar manner as reported earlier for DCF [14].

The position of nitro and nitroso groups in the molecules of TPDCF340 and TPDCF324 was confirmed by synthetized standards [38]. However, due to the lack of standards for the other TPs, we could not confirm the exact position of the nitro and nitroso groups. However, we proposed the NO group attached to the nitrogen of the diphenilinic moiety (i.e. N-nitroso derivative) as DCF was transformed in our previous publication [14].

The detection of two peaks of two isomers of TPMCF340a and c, ($C_{14}H_9Cl_2N_2O_4$), suggested that the incorporation of NO_2 into MCF ($C_{14}H_{10}Cl_2NO_2$) occurred at different sites of the molecule (see structures proposed in figure 2). Given the steric hindrance phenyl ring discussed in the previous section, nitration was deemed more likely to the isomers observed for TPFFN326 ($C_{14}H_8F_3N_2O_4$), TPTFM306 ($C_{14}H_{10}ClN_2O_4$) and TPMFN286 ($C_{15}H_{13}N_2O_4$). Even though fragmentation pattern was the same as that observed for TPDCF340, in either case the diagnostic ion corresponding to the loss of NO_2 could not be detected. The whole fragmentation pattern for the nitro-derivative of DCF (TPDCF340) had already been described in our group with Q-ToF-MS [14]. Despite this diagnostic ion for the presence of an NO_2 group in the molecule of TPDCF340 could not be detected in this experiment, the derivative was confirmed with synthetized standard [29]. For the nitroso-TPs tentatively identified, it was assumed that the mass difference in +30 Da with respect to the parent compound corresponded to incorporation of a NO group into the molecule. Such hypothesis was confirmed by MS^2 spectra, with diagnostic ion corresponding to the loss of NO identified in all cases (i.e., TPDCF324, TPMCF324, TPFFN310, TPTFM290 and TPMFN270). In the case of nitro-derivatives, the mass differences observed of +46 Da and +16 Da compared to parent compound and nitroso-TP, respectively, were tentatively assigned to the inclusion of an NO_2 group into the molecule of the parent compound. Thus, we proposed the same nitro-transformations for MCF, MEF, FFN, TFM and DCF. As it is shown in Figures A.3-A.7, we tentatively assigned the fragmentation pathways observed for these isomers (see Table A-1 and detailed description in SM) to the chemical structures of isomers a and c for nitro-MCF (TPMCF340); b and c of nitro-MFN (TPMFN270), nitro-FFN (TPFFN), and nitro-TFM (TPTFM) where C-nitration would occur at any position of the phenyl ring bearing the carboxylic moiety.

In light of these observations, the chemical synthesis of the postulated TPs, as it was previously performed for the nitro- and nitroso- TPs of DCF, would be ultimately required in order to confirm their structure.

3.3.2 Mechanisms of biotransformation and biodegradability of DCF and related NSAIDs in the different nitrifying activated sludge batch reactors

Nitrifiers involved in biotransformation of NSAIDs

We proposed that the NSAIDs underwent minor modifications of their structure via nitrosation and nitration biotransformation reactions mediated by the nitrifying microbial community present in the NAS. Although the contribution of nitrifiers to the biomass in the mixed microbial community of the activated sludge tank in WWTPs is less than 5 % [40], the operational conditions of the lab-scale reactors were favourable for the growth of nitrifiers in terms of NH_3 and oxygen supply, temperature (20-22 ºC) and pH (7.4±0.3), of the mixed liquor.

Three controlled experimental approaches were used to determine the importance of nytrifiers for NSAIDs biotransformation: i) a biotic reactor (R1) to evaluate biotransformation capabilities of different nitrifying microorganisms, including ammonia-oxidizing microorganisms and nitrite-oxidizing microorganisms ; ii) a second biotic reactor (R2) to identify possible differences in NSAIDs biotransformation pathways treated with ATU inhibitors of ammonia oxidation; and iii) a third reactor (R3) to investigate the non-microbial mediated transformation of NSAIDs in the nitrifying activated sludge after inhibition of microorganisms with SA. Additionally, only in the case of DCF, a iv) fourth reactor was tested to evaluate the possible transformation of this recalcitrant compound under starvation conditions of nitrifiers in non-enriched ammonia sludge.

Biotransformation-time profiles for the parent compounds and their nitrogen-TPs (+30 and +46 Da; nitroso and nitro-TPs, respectively) are shown in Figure 4 and Figures A-8 to A-12. Overall, parent compounds showed different biotransformation patterns, with the exceptions of DCF (in R1-biotic and R3-SA) and MCF (in R1-biotic and R2-ATU). Nitroso- and nitro- TPs were detected in all batch reactors. However, relative amount of TP observed differed among NSAIDs and treatments.

Enhanced biodegradation of pharmaceuticals under nitrifying conditions has been commonly related to the activity of AOB which may co-metabolize these compounds using ammonia monooxygenase enzymes, responsible for ammonia oxidation [9,33,34,41,42]. However, AOA also contribute, producing ammonia monooxygenase as well, to ammonia oxidation in the nitrifying reactors [9,43]. Ammonia monooxygenase directly transforms organic compounds primarily via hydroxylation, while reactive nitrogen species (hydroxylamine (NH_2OH), nitrite (NO_2^-), and nitric oxide (NO)) can trigger significant chemical transformations of organic compounds through nitration, hydroxylation, and deamination [9]. According to the review of Su et al., [9], DCF

382 and the fenamates investigated can undergo through microbial mediated transformations and yield
383 the TPs tentatively identified either by ammonia monooxygenase and reactive nitrogen species, as
384 their chemical structures contained substituted aromatic rings and secondary amines.

385 ATU is considered a specific inhibitor of ammonia monooxygenase produced by AOB and
386 has been frequently used to evidence the linkage between biotransformation of contaminants and
387 nitrification mediated by AOB [33,41]. In previous works [33,41], the activity of AOB was fully
388 inhibited by ATU, null removal of parent compounds was observed and no TPs were identified. In
389 this study, instead, we observed removal and biotransformation in batch reactors treated with ATU
390 (R2). However, in most of previous studies the amount of ATU added to the mixed liquor was up to
391 5-fold higher than the spiking level in our batch-reactors [33,41]. Such inhibition was expected to
392 account for autotrophs and thus minor biodegradation could only be due to heterotrophs using the
393 methanol solvent of NSAIDs spike as a substrate [41]. Depending on the conditions in the sludge,
394 AOA might also coexist with AOB, playing an important role in nitrogen removal from wastewater
395 [43]. AOA are highly tolerant to ATU, which was not as effective inhibitor as it is for AOB [44].
396 Indeed, while low concentrations of ATU have a strong effect on AOB, higher levels (11,619 mgL^{-1})
397 of ATU are required for complete inhibition of AOA [43]. Thus, biotransformation of NSAIDs
398 observed in R2 batch-reactors may account also for AOA. Full inhibition of ammonia
399 monooxygenase enzymes activity achieved in reviewed studies would be due to the high
400 concentration of ATU, which could have been enough to inhibit, as well the less abundant AOA, in
401 the nitrifying activated sludge cultures. We found only one work in the literature in which ATU was
402 added at our same spiking-level, and it demonstrated that after AOB inhibition, AOA nitrifying
403 activity is enhanced. [45]. AOA are more resilient in extreme conditions (such as low temperature
404 and low oxygen level) than AOB [45]. Thus, the formation of nitroso and nitro-TPs in batch-reactors
405 R2 (Figures A-8a to A-12a) and R3 (Figures A-8b to A-12b) as well, could have been microbially
406 mediated by AOA. SA is an aerobic and anoxic respiration inhibitor, expected to hamper ammonia
407 and nitrite oxidation in the nitrifying activated sludge [46]. Apparently, 10 mgL^{-1} of SA added would
408 not have been enough to fully eliminate the ammonia-oxidizing microorganisms in batch-reactor
409 R3. Since ATU is an specific inhibitor for ammonia monooxygenase enzyme rather than nitrite
410 oxidoreductase enzyme, NOB were neither inhibited [10]. Hence, nitroso and nitro-TPs observed
411 might be due to oxidation of residual nitrite in the nitrifying activated sludge by NOB. In fact,
412 despite reducing their ammonia-oxidizing activity, AOB and AOA can accumulate ammonia
413 monooxygenase enzymes in the absence of ammonia [45]. These autotrophic ammonia-oxidizing
414 microorganisms are able to survive and recover after long-term starvation conditions. Thus,
415 ammonia-starvation kept in R4 might not have affected AOA, which could have been eventually
416 involved in DCF biotransformation observed (Figure A-8c).

417 Summarizing, the type and concentration of the inhibitors added and conditions kept in
418 batch-reactors R2-R4 might not have been enough to efficiently reduce the activity of AOMs and

nitrite-oxidizing microorganisms communities. Alternative hypothesis could be that biodegradation of parent compounds and formation of nitroso and nitro-TPs from other microorganisms present in the nitrifying activated sludge recovered or NSAIDs were also removed due to other microorganisms, such as heterotrophic nitrifiers or commamox [12]. Based on the evidence of live cells in the nitrifying activated sludge of every microcosm (i.e. bioreactors R1-R4) measured (Figure A-13 and more detailed results description in SM), we postulate that removal of NSAIDs and their transformation observed 63-days biodegradation experiment were microbially mediated processes. The ratio of Live/Dead (L/D) bacteria cells in activated sludge was determined at the stable stage and detailed results are described in SM (Table A-2 and Figure A.14). Despite the more effective inhibition (L/D = 0.28) was measured in batch reactor R3, we detected ~2×10^8 live cells indicating that microbial respiration was not fully suppressed. This would explain biodegradation of NSAIDs and formation of their nitrogen-TPs observed in R3. Contrarily to our expectations, L/D and/or the number of live bacteria cells were higher in microcosms where AOB were supposed to be inhibited (R2), compared to those not inhibited (R1). Indeed, L/D determined in bioreactor R1 spiked with MCF evidenced more effective inactivity compared to measures in R2, as a considerably higher number of dead bacteria cells was counted compared to the live cells. Interestingly, starvation conditions kept in bioreactor R4 fortified with DCF did not seem to affect microbial community, since L/D were similar to those calculated for R2 and R1 and the number of live and dead bacteria cells was at the same level of those measured in R1. However, though NSAIDs showed to be biodegradable, the responsible bacterial species were not investigated. Thus, the role of both autotrophic and heterotrophic nitrifiers in the nitroso- and nitro-transformation processes of selected NSAIDs could not be clarified. Neither abundance and composition nor microbial community activity was assessed during the performance of our experiments, thus all our hypotheses could only be disentangled in further investigation including microbiological and genomics analyses.

Despite microbial activity could be notably reduced under conditions held in microcosms R2-R4, degradation of NSAIDs and their transformation into nitrogen-derivatives could also be the result of abiotic reactions with enzymes-mediated ammonia oxidation by ammonia monooxygenase intermediates accumulated in the sludge, such as hydroxylamine [12], free nitrite or free nitrous acid (FNA) [31,34]. Therefore, future experiments aimed at exploring biodegradation removal should be controlled by a neutral pH condition without nitrite accumulation, in order to account for hydroxylamine or FNA-mediated nitroso- and nitro- transformation of DCF and structural analogues.

Eventually, we conjectured the uncontrolled transformation of NSAIDs during storage of samples at -20 ºC. Despite 5% of MeOH was added to all sample extracts before storage to hamper microbial activity, the decrease of pH in solution in presence of nitrite concentrations could have favored the abiotic transformation of the NSAIDs investigated [31]. This could explain the

residual levels of nitrogen-TPs identified, particularly in samples collected from batch-reactor R3 even at the earliest monitoring days.

Removal of NSAIDs

Removal of NSAIDs and percentages of formation of nitrogen-derivatives identified are summarized in Table A-3 and described in detail in SM. MFN, FFN and TFM were efficiently removed (99%) than DCF with different conditions kept in batch-reactors. On the other hand, DCF and MCF showed a more recalcitrant behavior with removals of ≤51% under full nitrification (R1) and SA addition (R3). Unexpectedly, the most efficient biodegradation of NSAIDs was observed with ATU addition (R2), for which the maximum removal of DCF increased up to 87%. Likewise, contrarily to our expectations, the more biodegradable fenamates were efficiently removed as well in batch-reactor R3 and only DCF and MCF were affected by the addition of SA. Overall, MFN showed the higher biodegradation rates, followed by FFN, TFM, DCF and MCF. While MFN, FFN, TFM and DCF disappeared gradually in the time-line series of both R1 and R2, a general steady-state of removal was observed for MCF. The most evident effect of respiration inhibition by the addition of SA was the slower biodegradation rate compared to those observed in microcosms R1 and R2. However, MFN, FFN and TFM confirmed their highly biodegradable nature, as their removal rates recovered towards the end of the experiment in R3.

Biodegradation trends of NSAIDs investigated evolved in agreement with their nitroso and nitro-transformation profiles (Figures A-8 to A-12). In fact, the maximum total percentages of formation for nitrogen-TPs of NSAIDs were 31% and 28% for TPMFN270 and TPFFN310 in R1, 34% and 20% for TPMFN270 and TPFFN310 in R2; and 16% and 11%, for TPMFN270 and TPMCF340c in R3 (Table A-3). The formation efficiencies of nitroso and nitro-derivatives are described in detail in the SM. Due to the lack of standards for TPs identified, we could not compare the efficiency of nitroso or nitro biotransformation among fenamates, as we could not account for the response intensity of every compound under analytical conditions used.

As reported in previous studies [33,34,41,47], we proved that enhanced nitrifying conditions foster the biotransformation efficiencies of DCF and fenamates investigated. Recently, higher kinetic biodegradation rates of pharmaceuticals were observed in nitrifying activated sludge cultures under full nitrification conditions compared to the kinetics observed in microcosms with ATU addition [34]. The role of AOB in pharmaceuticals biotransformation mainly due to the co-metabolic biodegradation was considered as the main reason for the different behaviour. Diversely, we observed similar kinetics between batch-reactors R1 and R2, and despite biodegradation rates were slower we also observed nitrosation and nitration processes in R2. These trends suggested that AOB might not be the only nitrifiers involved in the biotransformation of NSAIDs investigated. Moreover, nitrifying activated sludge may show a different affinity for each NSAID, probably due to steric hindrance, as it was previously conjectured for APAA and DCF comparison, activation

energy limitations or the presence of specific functional groups [41,47]. The recalcitrance of pharmaceuticals to be degraded by ammonia monooxygenase enzymes in nitrifying activated sludge cultures was linked to the presence of halogens and aromatic amines in their chemical structures [41]. All NSAIDs investigated share a canonical chemical structure of an N-phenylanthranilic acid with different groups (i.e., -F, -Cl, -CH_3) substituting hydrogens of the of the N-phenyl ring at different positions. The high removals observed for all compounds investigated, despite featuring halogens and aromatic amine structure, suggests again that their biodegradability would not only account for AOBs present in the nitrifying activated sludge but also for other microorganisms. Under different conditions in nitrifying activated sludge cultures, biodegradability of NSAIDs investigated was in the following order: MFN < FFN < TFM < DCF < MCF. Having a look into their corresponding chemical structures (Figure 1), the readily biodegradable nature of MFN could be explained by the minimal steric hindrance of the N-phenyl moiety, which would ease the approach of reactive nitrogen species to initiate nitrosation or nitration of the molecule. According to former hypotheses [41], the transformation mechanisms and biodegradability of FFN and TFM would be hampered by the presence of fluorine and chlorine atoms. However, given the location of the halogenated substituents, the approach of reactive nitrogen species would still occur favourably on the opposite sites of the halogenated groups. On the contrary, as discussed previously (section 3.2), the substitution sites of two chlorine atoms in the molecules of DCF and MCF could explain their more recalcitrant nature and the higher relative abundance of their nitro-TPs, compared to their nitroso-TPs.

While the formation of nitroso-TPs increased gradually up to maximum percentages determined towards the end of experiment in R1 and R2 (Figures 4 and A-8 to A-12); these were almost completely degraded in R3 (Figures A8-A12). Re-appearance of all parent compounds was observed towards the last third-part of the experiment in R1 (Figure 4). These trends might suggest mechanisms of retransformation of poorly stable TPs back to their parent compound under long-term biodegradation in nitrifying activated sludge. To gain further confidence on this conjecture, we evaluated the correlations between levels of parent compound and TPs (Table A-4). Regarding nitroso-TPs, DCF levels showed high negative correlation with the concentration of TPDCF324 along the whole biodegradation experiment in both microcosms R1, R2 and R3. FFN, TFM and MFN showed the same behavior with TPFFN310, TPTFM290 and TPMFN270, respectively, in R1 and R2. These negative relationships explain that levels of nitroso-TPs increase with the decrease of parent compound and the opposite way, the levels of DCF, FFN, TFM and MFN increased again towards the end of the biodegradation experiment with the decrease of TPDCF324, TPFFN310, TPTFM290 and TPMFN270, respectively. The strong relationships observed for DCF, TFM, MFN and their corresponding nitroso-TPs (Table A-4) support the hypothesis of retransformation of TP back to and its parent compound. As for nitro-TPs, TPDCF340, TPFFN326c, TPTFM306a, TPTFM306b, TPMFN286a and TPMFN286b showed significant negative correlation with their parent compound in R1, while in R2 were significant for TPFFN326a, TPFFN326c, TPTFM306a,

TPTFM306b, TPMFN286a and TPMFN286b; and only TPFFN326a and TPMFN286b in R3. As observed for nitroso-TPs, the decrease of parent compounds explains the increase of nitro-TPs. Overall, nitro-TPs showing negative relationships with their parent compounds had positive correlation with nitroso-TPs, indicating that both nitrogen-derivatives were products of fenamates studied. On the other hand, TPMCF340c, TPFFN326b, TPTFM306c and TPMFN286c showed strong positive correlation with their parent compound in all mesocosms. The same nitro-TPs showed significant correlation with respective TPMCF324, TPFFN310, TPTFM290 and TPMFN280, suggesting that TPMCF340c, TPFFN326b, TPTFM306c and TPMFN286c could be triggered by further transformation of nitroso-TPs. This hypothesis would be supported by the significant negative correlations observed TPTFM306c and TPMFN286c with their respective isomers b and c, which would be triggered by TFM and MFN. Isomers c would be product of further transformation of nitroso-TPs or alternatively, derived from the spatial rearrangement of the nitro group in the molecule. We did also observe the increase of some parent compounds during the first hours of the biodegradation experiment and later recovery up to maximum levels, which were assigned to initially spiked concentrations. Such behavior was initially explained as incomplete dilution of standards spiked but could also be due to reversible biotransformation of the NSAIDs studied from their corresponding TPs already present in the nitrifying activated sludge culture.

4. Conclusions

In this work we have reported the discovery of unusual microbial nitration/nitrosation TPs of related NSAIDs of DCF in reactors amended with mixed liquor of WWTP.

- We identified ^{15}N-nitroso and ^{15}N-nitro DCF TPs in HRMS spectra obtained from bioreactors spiked with DCF and enriched with isotopically labelled (^{15}N) ammonia. These results provide evidence of the microbially mediated N-nitrosation and C-nitration of DCF, where nitrifiers would metabolize ^{15}N-NH_4 triggering ^{15}N-N RNS eventually involved in the biotransformation of DCF.
- HRMS^n analysis in extracts collected from nitrifying activated sludge bioreactors spiked with DCF structurally related fenamates, namely APAA, MCF, FFN, TFM, and MFN, allowed to identify fragmentation patterns suggesting incorporation of NO group into the diphenylamine and carboxylic (this only in the case of DCF and MCF) moieties of the parent compounds. Formation of nitro-TPs was also suggested based on observed mass differences in +46 Da.
- We evidenced nitroso- and nitro-transformation of DCF and its structural analogues occurring not only under nitrifying activated sludge conditions, but also in incubations after selective inhibition of AOB, nitrifiers starvation and even complete inhibition of microorganisms. According to these observations, more resilient AOA and nitrite-oxidizing

568 microorganisms coexisting with AOB in the bioreactors would have played an important role
569 in NSAIDs biodegradation and transformation.

570 • We demonstrated that biodegradability of DCF and analog fenamates studied is hampered
571 by the presence of halogens and aromatic amines but can be enhanced by microbial
572 mediation of the nitrifying microbial community present in the activated sludge. The re-
573 appearance of NSAIDs studied in removal and biotransformation profiles suggested the
574 secondary biotransformation of TPs identified back to their parent compounds.

575 Provided the occurrence of NO/NO_2 DCF derivatives in WWTPs and SW reported in previous
576 works we propose the additional nitration/nitrosation TPs of DCF and related NSAIDs tentatively
577 identified in this work to be included in following monitoring of WWTPs and receiving SW bodies.
578 Considering that pharmaceuticals may undergo further microbial biodegradation once released into
579 water bodies, follow-up studies should also investigate the natural formation of NO/NO_2 derivatives
580 in the aquatic environment. Considering the evidence reporting the toxicity of photo-TPs of DCF,
581 the toxicity assessment on these TPs would be equally relevant to define their potential
582 toxicological effects on aquatic ecosystems. Finally, further research should be focused on the
583 characterization of microbial communities responsible for the biotransformation of these
584 pharmaceuticals to improve removal efficiency in WWTPs.

585

586 **Appendix A. Supplementary material**

587 Supplementary data associated with this article shows Tables A-1 to A-4 and Figures A-1 to A-14
588 and additional descriptions of NSAIDs investigated, and TPs identified.

589

590 **Acknowledgements**

591 This study has been financially supported by the EU through the PRIMA project (INWAT
592 201980E121). This work was supported by the Spanish Ministry of Science and Innovation (Project
593 CEX2018-000794-S). Thermofisher are also acknowledged for their technical support with the
594 Orbitrap software.

595

596 **References**

597 [1] A. Belloni, D. Morgan, V. Paris, Pharmaceutical Expenditure And Policies: PAST TRENDS
598 AND FUTURE CHALLENGES, (2016) 1–75. https://doi.org/10.1787/18152015.

599 [2] B. shu He, J. Wang, J. Liu, X. min Hu, Eco-pharmacovigilance of non-steroidal anti-
600 inflammatory drugs: Necessity and opportunities, Chemosphere. 181 (2017) 178–189.
601 https://doi.org/10.1016/j.chemosphere.2017.04.084.

[3] E.N. Evgenidou, I.K. Konstantinou, D.A. Lambropoulou, Occurrence and removal of transformation products of PPCPs and illicit drugs in wastewaters: A review, Sci. Total Environ. 505 (2015) 905–926. https://doi.org/10.1016/j.scitotenv.2014.10.021.

[4] C.G. Daughton, Pharmaceuticals in the environment: Sources and their management, 2nd ed., Elsevier B.V., 2013. https://doi.org/10.1016/B978-0-444-62657-8.00002-1.

[5] L. Sabater-Liesa, N. Montemurro, A. Ginebreda, D. Barceló, P. Eichhorn, S. Pérez, Retrospective mass spectrometric analysis of wastewater-fed mesocosms to assess the degradation of drugs and their human metabolites, J. Hazard. Mater. 408 (2021). https://doi.org/10.1016/j.jhazmat.2020.124984.

[6] A. Jelic, M. Gros, A. Ginebreda, R. Cespedes-Sánchez, F. Ventura, M. Petrovic, D. Barcelo, Occurrence, partition and removal of pharmaceuticals in sewage water and sludge during wastewater treatment, Water Res. 45 (2011) 1165–1176. https://doi.org/10.1016/j.watres.2010.11.010.

[7] B. Petrie, R. Barden, B. Kasprzyk-Hordern, A review on emerging contaminants in wastewaters and the environment: Current knowledge, understudied areas and recommendations for future monitoring, Water Res. 72 (2015) 3–27. https://doi.org/10.1016/j.watres.2014.08.053.

[8] K.M. Onesios, J.T. Yu, E.J. Bouwer, Biodegradation and removal of pharmaceuticals and personal care products in treatment systems: A review, Biodegradation. 20 (2009) 441–466. https://doi.org/10.1007/s10532-008-9237-8.

[9] Q. Su, A.-R. Schittich, M.M. Jensen, H. Ng, B.F. Smets, Role of Ammonia Oxidation in Organic Micropollutant Transformation during Wastewater Treatment: Insights from Molecular, Cellular, and Community Level Observations, Environ. Sci. Technol. (2021). https://doi.org/10.1021/acs.est.0c06466.

[10] B.B. Ward, Nitrification, Encycl. Ecol. 2 (2018) 351–358. https://doi.org/10.1016/B978-0-12-409548-9.00697-7.

[11] P. Pjevac, C. Schauberger, L. Poghosyan, C.W. Herbold, M.A.H.J. van Kessel, A. Daebeler, M. Steinberger, M.S.M. Jetten, S. Lücker, M. Wagner, H. Daims, AmoA-targeted polymerase chain reaction primers for the specific detection and quantification of comammox Nitrospira in the environment, Front. Microbiol. 8 (2017) 1–11. https://doi.org/10.3389/fmicb.2017.01508.

[12] Y. Yu, P. Han, L.J. Zhou, Z. Li, M. Wagner, Y. Men, Ammonia Monooxygenase-Mediated Cometabolic Biotransformation and Hydroxylamine-Mediated Abiotic Transformation of Micropollutants in an AOB/NOB Coculture, Environ. Sci. Technol. 52 (2018) 9196–9205. https://doi.org/10.1021/acs.est.8b02801.

637 [13] L. Chimie, A. Universite, Nitration Processes of Acetaminophen in Nitrifying Activated
638 Sludge, 44 (2010) 284–289. https://doi.org/10.1021/es902129c.

639 [14] S. Pérez, D. Barceló, First evidence for occurrence of hydroxylated human metabolites of
640 diclofenac and aceclofenac in wastewater using QqLIT-MS and QqTOF-MS, Anal. Chem. 80
641 (2008) 8135–8145. https://doi.org/10.1021/ac801167w.

642 [15] V. Osorio, J. Sanchís, J.L. Abad, A. Ginebreda, M. Farré, S. Pérez, D. Barceló, Investigating
643 the formation and toxicity of nitrogen transformation products of diclofenac and
644 sulfamethoxazole in wastewater treatment plants, J. Hazard. Mater. 309 (2016) 157–164.
645 https://doi.org/10.1016/j.jhazmat.2016.02.013.

646 [16] S. Chiron, C. Duwig, Biotic nitrosation of diclofenac in a soil aquifer system (Katari
647 watershed, Bolivia), Sci. Total Environ. 565 (2016) 473–480.
648 https://doi.org/10.1016/j.scitotenv.2016.05.048.

649 [17] M. Brienza, C. Duwig, S. Pérez, S. Chiron, 4-nitroso-sulfamethoxazole generation in soil
650 under denitrifying conditions: Field observations versus laboratory results, J. Hazard. Mater.
651 334 (2017) 185–192. https://doi.org/10.1016/j.jhazmat.2017.04.015.

652 [18] M. Brienza, R. Manasfi, S. Chiron, Relevance of N-nitrosation reactions for secondary
653 amines in nitrate-rich wastewater under UV-C treatment, Water Res. 162 (2019) 22–29.
654 https://doi.org/10.1016/j.watres.2019.06.055.

655 [19] L. Lonappan, S.K. Brar, R.K. Das, M. Verma, R.Y. Surampalli, Diclofenac and its
656 transformation products: Environmental occurrence and toxicity - A review, Environ. Int. 96
657 (2016) 127–138. https://doi.org/10.1016/j.envint.2016.09.014.

658 [20] Y. Yang, Y.S. Ok, K.H. Kim, E.E. Kwon, Y.F. Tsang, Occurrences and removal of
659 pharmaceuticals and personal care products (PPCPs) in drinking water and water/sewage
660 treatment plants: A review, Sci. Total Environ. 596–597 (2017) 303–320.
661 https://doi.org/10.1016/j.scitotenv.2017.04.102.

662 [21] L.M. Madikizela, S. Ncube, L. Chimuka, Uptake of pharmaceuticals by plants grown under
663 hydroponic conditions and natural occurring plant species: A review, Sci. Total Environ. 636
664 (2018) 477–486. https://doi.org/10.1016/j.scitotenv.2018.04.297.

665 [22] B. Bonnefille, E. Gomez, F. Courant, A. Escande, H. Fenet, Diclofenac in the marine
666 environment: A review of its occurrence and effects, Mar. Pollut. Bull. 131 (2018) 496–506.
667 https://doi.org/10.1016/j.marpolbul.2018.04.053.

668 [23] T.H. Miller, N.R. Bury, S.F. Owen, J.I. MacRae, L.P. Barron, A review of the pharmaceutical
669 exposome in aquatic fauna, Environ. Pollut. 239 (2018) 129–146.
670 https://doi.org/10.1016/j.envpol.2018.04.012.

[24] C.I.D. (Eu) 2015/495, of 20 M. 2015, COMMISSION IMPLEMENTING DECISION (EU) 2015/495 of 20 March 2015 establishing a watch list of substances for Union-wide monitoring in the field of water policy pursuant to Directive 2008/105/EC of the European Parliament and of the Council, Off. J. Eur. Union. L78/40 (2015) 20–30. https://doi.org/http://eur-lex.europa.eu/pri/en/oj/dat/2003/l_285/l_28520031101en00330037.pdf.

[25] EU Decision 2018/840, COMMISSION IMPLEMENTING DECISION (EU) 2018/840 of 5 June 2018, Off. J. Eur. Union. 141 (2018) 9–12.

[26] M. Schmitt-Jansen, P. Bartels, N. Adler, R. Altenburger, Phytotoxicity assessment of diclofenac and its phototransformation products, Anal. Bioanal. Chem. 387 (2007) 1389–1396. https://doi.org/10.1007/s00216-006-0825-3.

[27] G.Š. Parezanović, M. Lalic-Popovic, S. Golocorbin-Kon, V. Vasovic, B. Milijašević, H. Al-Salami, M. Mikov, Environmental Transformation of Pharmaceutical Formulations: A Scientific Review, Arch. Environ. Contam. Toxicol. 77 (2019) 155–161. https://doi.org/10.1007/s00244-019-00630-z.

[28] V. Osorio, J. Sanchís, J.L. Abad, A. Ginebreda, M. Farré, S. Pérez, D. Barceló, Investigating the formation and toxicity of nitrogen transformation products of diclofenac and sulfamethoxazole in wastewater treatment plants, J. Hazard. Mater. 309 (2016). https://doi.org/10.1016/j.jhazmat.2016.02.013.

[29] V. Osorio, M. Imbert-Bouchard, B. Zonja, J.L. Abad, S. Pérez, D. Barceló, Simultaneous determination of diclofenac, its human metabolites and microbial nitration/nitrosation transformation products in wastewaters by liquid chromatography/quadrupole-linear ion trap mass spectrometry, J. Chromatogr. A. 1347 (2014) 63–71. https://doi.org/10.1016/j.chroma.2014.04.058.

[30] T.A. Heinrich, R.S. Da Silva, K.M. Miranda, C.H. Switzer, D.A. Wink, J.M. Fukuto, Biological nitric oxide signalling: Chemistry and terminology, Br. J. Pharmacol. 169 (2013) 1417–1429. https://doi.org/10.1111/bph.12217.

[31] K.S. Jewell, A. Wick, T.A. Ternes, Comparisons between abiotic nitration and biotransformation reactions of phenolic micropollutants in activated sludge, Water Res. 48 (2014) 478–489. https://doi.org/10.1016/j.watres.2013.10.010.

[32] K. Nödler, T. Licha, M. Barbieri, S. Pérez, Evidence for the microbially mediated abiotic formation of reversible and non-reversible sulfamethoxazole transformation products during denitrification, Water Res. 46 (2012) 2131–2139. https://doi.org/10.1016/j.watres.2012.01.028.

[33] E. Kassotaki, G. Buttiglieri, L. Ferrando-Climent, I. Rodriguez-Roda, M. Pijuan, Enhanced

sulfamethoxazole degradation through ammonia oxidizing bacteria co-metabolism and fate of transformation products, Water Res. 94 (2016) 111–119. https://doi.org/10.1016/j.watres.2016.02.022.

[34] G. Wu, J. Geng, S. Li, J. Li, Y. Fu, K. Xu, H. Ren, X. Zhang, Abiotic and biotic processes of diclofenac in enriched nitrifying sludge: Kinetics, transformation products and reactions, Sci. Total Environ. 683 (2019) 80–88. https://doi.org/10.1016/j.scitotenv.2019.05.216.

[35] M. Lahti, A. Oikari, Microbial transformation of pharmaceuticals naproxen, bisoprolol, and diclofenac in aerobic and anaerobic environments, Arch. Environ. Contam. Toxicol. 61 (2011) 202–210. https://doi.org/10.1007/s00244-010-9622-2.

[36] A. Langenhoff, N. Inderfurth, T. Veuskens, G. Schraa, M. Blokland, K. Kujawa-Roeleveld, H. Rijnaarts, Microbial removal of the pharmaceutical compounds ibuprofen and diclofenac from wastewater, Biomed Res. Int. 2013 (2013). https://doi.org/10.1155/2013/325806.

[37] V. Osorio, M. Imbert-Bouchard, B. Zonja, J.-L. Abad, S. Pérez, D. Barceló, Simultaneous determination of diclofenac, its human metabolites and microbial nitration/nitrosation transformation products in wastewaters by liquid chromatography/quadrupole-linear ion trap mass spectrometry, J. Chromatogr. A. 1347 (2014). https://doi.org/10.1016/j.chroma.2014.04.058.

[38] M. Barbieri, J. Carrera, C. Ayora, X. Sanchez-Vila, T. Licha, K. Nödler, V. Osorio, S. Pérez, M. Köck-Schulmeyer, M. López de Alda, D. Barceló, Formation of diclofenac and sulfamethoxazole reversible transformation products in aquifer material under denitrifying conditions: Batch experiments, Sci. Total Environ. 426 (2012). https://doi.org/10.1016/j.scitotenv.2012.02.058.

[39] P. Chen, W. Lv, Z. Chen, J. Ma, R. Li, K. Yao, G. Liu, F. Li, Phototransformation of mefenamic acid induced by nitrite ions in water: mechanism, toxicity, and degradation pathways, Environ. Sci. Pollut. Res. 22 (2015) 12585–12596. https://doi.org/10.1007/s11356-015-4537-0.

[40] P.H. Nielsen, T.R. Thomsen, J.L. Nielsen, Bacterial composition of activated sludge - Importance for floc and sludge properties, Water Sci. Technol. 49 (2004) 51–58. https://doi.org/10.2166/wst.2004.0606.

[41] E. Fernandez-Fontaina, I.B. Gomes, D.S. Aga, F. Omil, J.M. Lema, M. Carballa, Biotransformation of pharmaceuticals under nitrification, nitratation and heterotrophic conditions, Sci. Total Environ. 541 (2016) 1439–1447. https://doi.org/10.1016/j.scitotenv.2015.10.010.

[42] J. Park, N. Yamashita, G. Wu, H. Tanaka, Removal of pharmaceuticals and personal care products by ammonia oxidizing bacteria acclimated in a membrane bioreactor: Contributions

741 of cometabolism and endogenous respiration, Sci. Total Environ. 605–606 (2017) 18–25.
742 https://doi.org/10.1016/j.scitotenv.2017.06.155.

743 [43] P. Srithep, P. Pornkulwat, T. Limpiyakorn, Contribution of ammonia-oxidizing archaea and
744 ammonia-oxidizing bacteria to ammonia oxidation in two nitrifying reactors, Environ. Sci.
745 Pollut. Res. 25 (2018) 8676–8687. https://doi.org/10.1007/s11356-017-1155-z.

746 [44] Y. Men, S. Achermann, D.E. Helbling, D.R. Johnson, K. Fenner, Relative contribution of
747 ammonia oxidizing bacteria and other members of nitrifying activated sludge communities to
748 micropollutant biotransformation, Water Res. 109 (2017) 217–226.
749 https://doi.org/10.1016/j.watres.2016.11.048.

750 [45] G.M. Islam, P. Vi, K.A. Gilbride, Functional relationship between ammonia-oxidizing bacteria
751 and ammonia-oxidizing archaea populations in the secondary treatment system of a full-
752 scale municipal wastewater treatment plant, J. Environ. Sci. (China). 86 (2019) 120–130.
753 https://doi.org/10.1016/j.jes.2019.04.031.

754 [46] P. Ginestet, J.M. Audic, V. Urbain, J.C. Block, Estimation of nitrifying bacterial activities by
755 measuring oxygen uptake in the presence of the metabolic inhibitors allylthiourea and azide,
756 Appl. Environ. Microbiol. 64 (1998) 2266–2268.

757 [47] E. Fernandez-Fontaina, F. Omil, J.M. Lema, M. Carballa, Influence of nitrifying conditions on
758 the biodegradation and sorption of emerging micropollutants, Water Res. 46 (2012) 5434–
759 5444. https://doi.org/10.1016/j.watres.2012.07.037.

760

761 **Figure and Table captions**

762 **Figure 1.** Chemical structures of NSAIDS (parent compounds) investigated in batch experiments,
763 namely DCF, APAA, MCF, FFN, TFM and MFN.

764 **Figure 2.** (-)-HESI-MS/MS of (a) NO-DCF (TPDCF324) and (c) NO_2-DCF (TPDCF340) from a
765 bioreactor amended with NH_4-N; (b) ^{15}N NO-DCF (TPDCF324); and (d) ^{15}N NO_2-DCF (TPDCF340)
766 from a bioreactor amended with $^{15}NH_4$-N; and (e) APAA and (f) its tentatively proposed nitroso
767 derivative TPAPAA256 together with their chemical structures.

768 **Figure 3.** Chromatographic retention behaviour of parent compounds (open stars) and their
769 identified TPs (closed hexagons)

770 **Figure 4.** Qualitative biotransformation profiles of NSAIDs studied and its biotransformation
771 products i.e. nitrogen-TPs (+30 and +46 Da), in biodegradation experiments in nitrifying activated
772 sludge batch-reactor R1: (a) DCF, TPDCF324 and TPDCF340; (b) MCF, TPMCF324 and
773 TPMCF340; (c) TFM, TPTFM290 and TPTFM306; (d) FFN, TPFFN310 and TPFFN326; and (e)
774 MFN, TPMFN270 and TPMFN286. Qualitative evolution of levels of parent compound and TP are

represented as A/A_0 (%) (Y-axis) plotted against time course in hours of the biodegradation experiment (X-axis). Y-axis indicates the peak areas of the extracted ion chromatograms of parent compound or its TPs (A) normalized to the initial peak area of parent compound at maximum initial concentration (A_0) calculated as percentages.

Table 1. TP name, Retention time (min), elemental composition and exact mass of parent compounds and proposed TPs identified in bioreactors fortified separately with DCF, MCF, FFN, TFM, and MFN.

TP	Retention Time (min)	Elemental composition	Exact mass [*m/z*]
		DCF	
DCF	4.44	$C_{14}H_{11}Cl_2NO_2$	295.0167
TPDCF324	3.90	$C_{14}H_{10}Cl_2N_2O_3$	324.0063
TPDCF340	4.54	$C_{14}H_{10}Cl_2N_2O_4$	340.0012
		MCF	
MCF	4.86	$C_{14}H_{11}Cl_2NO_2$	295.0167
TPMCF324	3.84	$C_{14}H_{10}Cl_2N_2O_3$	324.0063
TPMCF340a	4.56	$C_{14}H_{10}Cl_2N_2O_4$	340.0012
TPMCF340c	4.97	$C_{14}H_{10}Cl_2N_2O_4$	340.0012
		FFN	
FFN	4.83	$C_{14}H_{10}F_3NO_2$	281.0664
TPFFN310	4.15	$C_{14}H_9F_3N_2O_3$	310.0560
TPFFN326a	4.64	$C_{14}H_9F_3N_2O_4$	326.0509
TPFFN326b	4.78	$C_{14}H_9F_3N_2O_4$	326.0509
TPFFN326c	5.00	$C_{14}H_9F_3N_2O_4$	326.0509
		TFM	
TFM	4.89	$C_{14}H_{12}ClNO_2$	261.0557
TPTFM290	4.03	$C_{14}H_{11}ClN_2O_3$	290.0453
TPTFM306a	4.60	$C_{14}H_{11}ClN_2O_4$	306.0402
TPTFM306b	4.71	$C_{14}H_{11}ClN_2O_4$	306.0402
TPTFM306c	5.00	$C_{14}H_{11}ClN_2O_4$	306.0402
		MFN	
MFN	4.75	$C_{15}H_{15}NO2$	241.1103
TPMFN270	3.76	$C_{15}H_{14}N_2O_3$	270.0999
TPMFN286a	4.38	$C_{15}H_{14}N_2O_4$	286.0948
TPMFN286b	4.56	$C_{15}H_{14}N_2O_4$	286.0948
TPMFN286c	4.83	$C_{15}H_{14}N_2O_4$	286.0948

Figure 1.

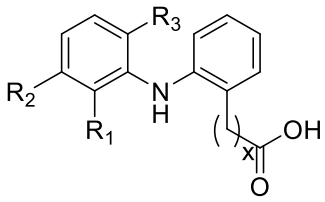

Compound	x	R1	R2	R3
DCF	1	Cl	H	Cl
APAA	1	H	H	H
FFN	0	H	CF_3	H
MCF	0	Cl	CH_3	Cl
MFN	0	CH_3	CH_3	H
TFM	0	CH_3	Cl	H

Figure

Click here to access/download;Figure;Osorio et al_Figure 2_Revised.docx

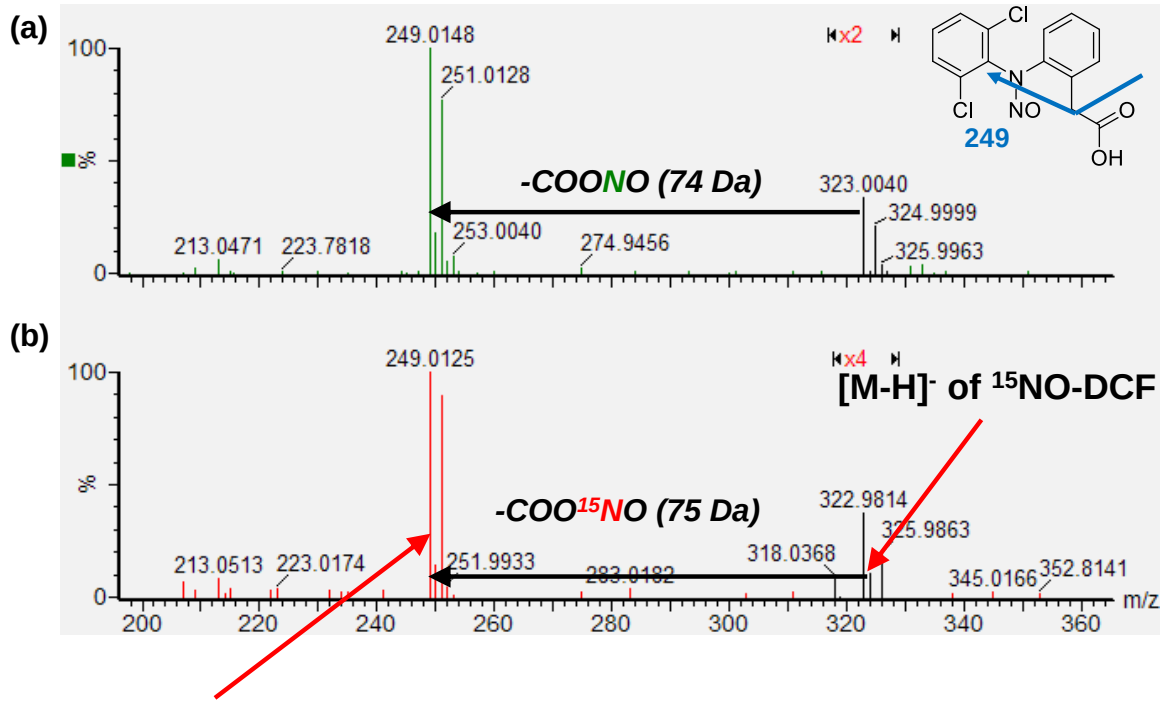

^{15}N-label lost with neutral fragment

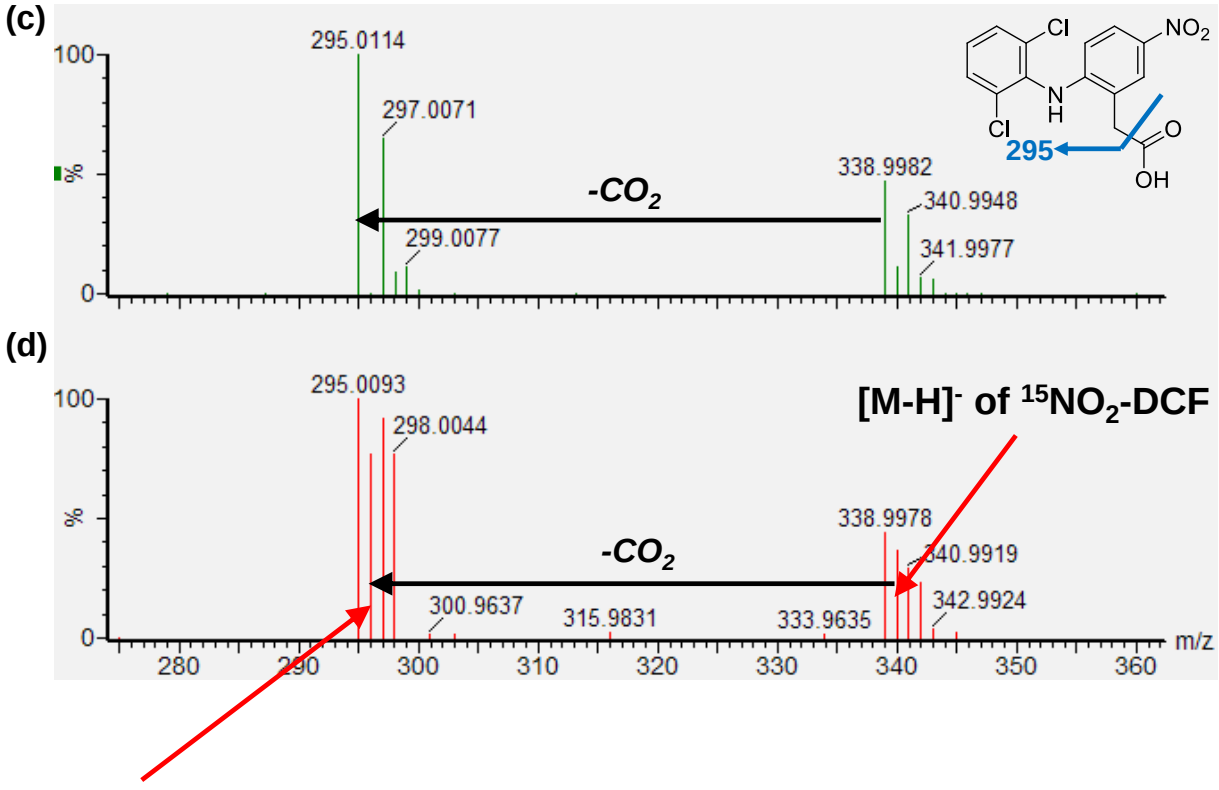

^{15}N-label still present in fragment ion

Figure

Click here to access/download;Figure;Osorio et al_Figure 3_Revised.docx

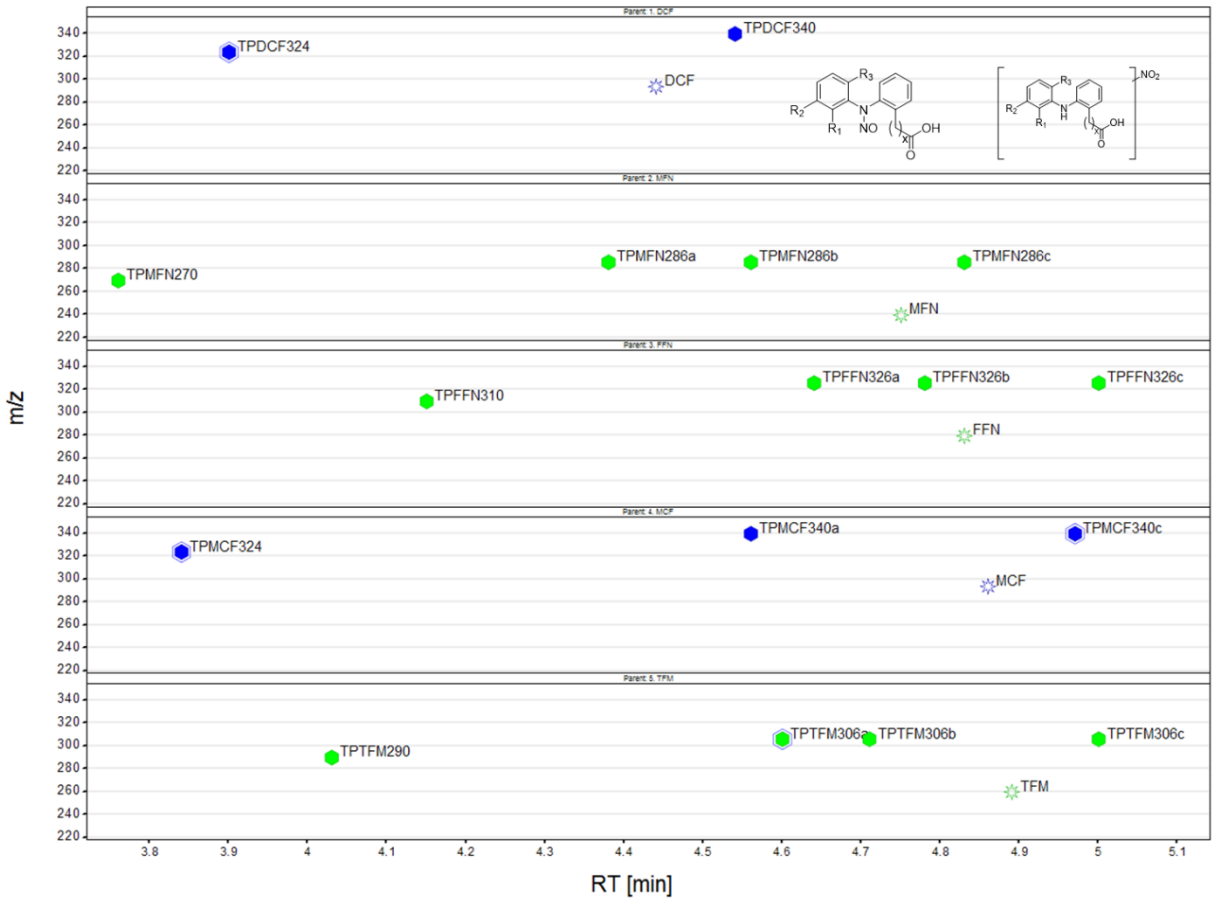

Figure

Click here to access/download;Figure;Osorio et al_Figure 4_Revised.docx

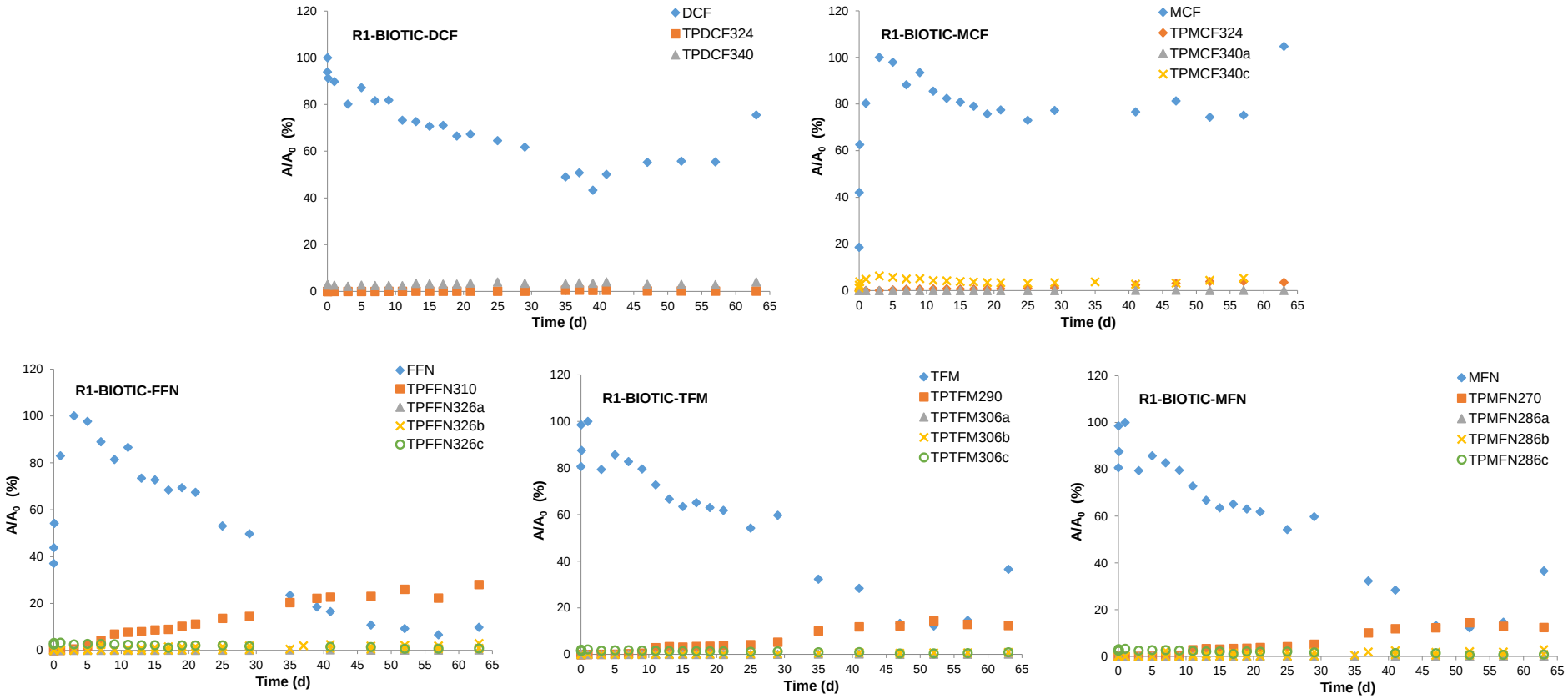

Supplementary material

Nitrosation and nitration of diclofenac and structurally related nonsteroidal anti-inflammatory drugs (NSAIDs) in nitrifying activated sludge

Victoria Osorio[1,2,3*], Alberto Cruz-Alcalde[1], Sandra Pérez[1]

[1] ENFOCHEM, IDAEA-CSIC, c/Jordi Girona 18-26, 08034 Barcelona (Spain).

[2] Catalan Institute for Water Research (ICRA), Emili Grahit 101, 17003 Girona, Spain

[3] and the Department of Chemistry, University of Girona, c/ Maria Aurèlia Capmany, 69, E-17003, Girona (Spain)

2. Materials and methods

2.1. Chemicals and standards

Diclofenac (IUPAC name: 2-(2-(2,6-dichlorophenylamino)phenyl)acetic acid) is an important nonsteroidal drug (NSAID) with anti-inflammatory, analgesic and antipyretic effects that is widely used for treatment of inflammation, pain, rheumatic diseases and to relieve fever. Among nonsteroidal anti-inflammatory drugs (NSAIDs), the group of fenamates contain fenamic acid (N-phenylanthranilic acid) as a core structural unit (Figure 1). Fenamates include Meclofenamic acid (MCF), Flufenamic acid (FFN), Tolfenamic acid (TFM) and Mefenamic acid (MFN). The chemical structure of DCF is closely related to fenamates, with a methylene (CH_2) separating the diphenylamine substructure from the acid moiety. In addition, the structurally related non-chlorinated compound 2-anilinophenylacetic acid (APAA), was studied in order to better understand the degradability of the NSAIDs.

3.2 Transformation of DCF and its non-chlorinated analogue

Figure A-1. Biotransformation profiles and extracted ion chromatograms acquired in negative ionization mode in bioreactor samples collected at different days of parent compound DCF and its nitro and nitroso-derivatives TPDCF340 and TPDCF324.

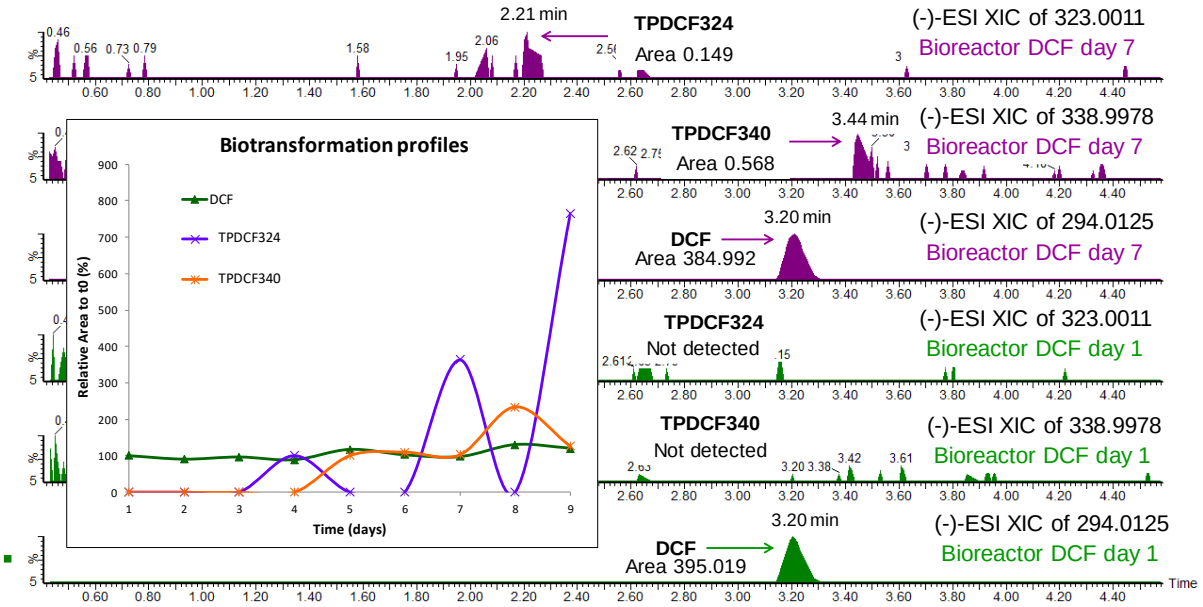

Figure A-2. Biotransformation profiles and extracted ion chromatograms acquired in negative ionization mode in bioreactor samples collected at different days of parent compound APAA s and its nitroso-derivative TPAPAA256.

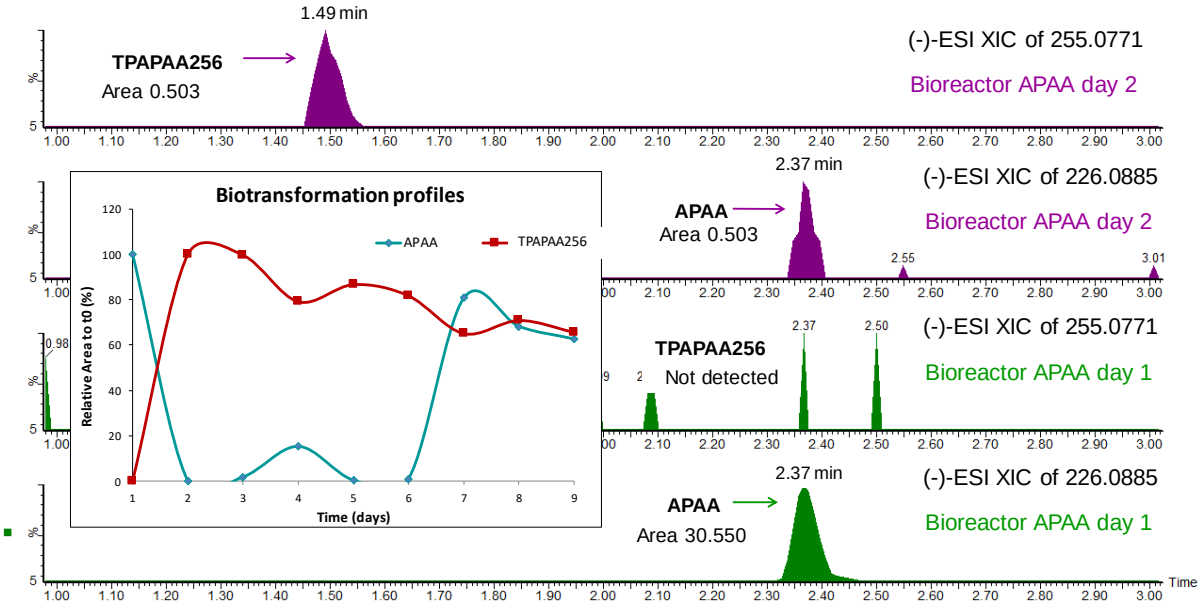

3.3 Transformation of DCF and four related fenamates

3.2.1 Identification and structural elucidation of TPs

Table A-1. Characterization of parent compounds and elucidated nitro and nitroso TPs. Fragmentation studies were performed in (-)-ESI mode: (a) DCF, TPDCF324 and TPDCF340; (b) MCF, TPMCF324 and the two isomers TPMCF340 a and c; (c) FFN, TPFFN310 and the three isomers TPFFN326a, b and c; (d) TFM, TPTFM290 and the three isomers TPTFM306 a, b and c; and (e) MFN, TPMFN270 and the three isomers TPMFN286 a, b and c.

(a)

Ion	Elemental composition	Exact mass [*m/z*]	Accurate mass [*m/z*]	Error [ppm]	DBE
$[M-H]^-$		**DCF**			
m/z 294	$C_{14}H_{10}Cl_2NO_2$	294.0094	294.0102	2.7	9.5
m/z 250	$C_{13}H_{10}Cl_2N$	250.0196	250.0195	-0.4	8.5
m/z 214	$C_{13}H_9ClN$	214.0429	214.0424	-2.3	9.5
m/z 178	$C_{13}H_8N$	178.0662	178.0654	-4.5	10.5
$[M-H]^-$		**TPDCF324**			
m/z 323	$C_{14}H_9Cl_2N_2O_3$	322.9996	322.9984	-3.7	10.5
m/z 279	$C_{13}H_9Cl_2N_2O$	279.0098	279.0096	-0.5	9.5
m/z 249	$C_{13}H_9Cl_2N$	249.0118	249.0114	1.1	9.0
m/z 245	$C_{13}H_8NO_2Cl$	245.0249	245.0241	1.2	10.0
m/z 228	$C_{13}H_7ONCl$	228.0211	228.0207	-1.7	10.5
m/z 200	$C_{12}H_7NCl$	200.0262	200.0256	-2.6	9.5
$[M-H]^-$		**TPDCF340**			
m/z 338	$C_{14}H_9Cl_2N_2O_4$	338.9945	338.9943	-0.6	10.5
m/z 295	$C_{13}H_9Cl_2\ N_2O_2$	295.0047	295.0045	-0.5	9.5
m/z 259	$C_{13}H_8ClN_2O_2$	259.0280	259.0128	0.0	10.5
m/z 229	$C_{13}H_8ClNO$	229.0300	229.0296	-1.7	10.0
m/z 174	$C_7H_7Cl_2N$	174.9961	174.9915	-26.3	

(b)

Ion	Elemental composition	Exact mass [*m/z*]	Accurate mass [*m/z*]	Error [ppm]	DBE
$[M-H]^-$		**MCF**			
m/z 294	$C_{14}H_{10}Cl_2NO_2$	294.0094	294.0095	0.3	9.5
m/z 250	$C_{13}H_{10}Cl_2N$	250.0196	250.0190	-2.4	8.5
m/z 214	$C_{13}H_9ClN$	214.0429	214.0421	-3.7	9.5

m/z 178	$C_{13}H_8N$	178.0662	178.0652	-5.6	10.5
$[M-H]^-$			**TPMCF324**		
m/z 323	$C_{14}H_9Cl_2N_2O_3$	322.9996	322.9995	-0.3	10.5
m/z 258	$C_{14}H_9ClNO_2$	258.0327	258.0323	-1.6	10.5
m/z 214	$C_{13}H_9ClN$	214.0429	214.0421	-3.7	9.5
m/z 174	$C_7H_7Cl_2N$	174.9961	174.9963	-1.7	4
$[M-H]^-$			**TPMCF340a**		
m/z 338	$C_{14}H_9Cl_2N_2O_4$	338.9945	338.9942	-0.9	10.5
m/z 295	$C_{13}H_9Cl_2N_2O_2$	295.0047	295.0047	0.0	9.5
m/z 259	$C_{13}H_8ClN_2O_2$	259.0280	259.0281	0.4	10.5
m/z 229	$C_{13}H_8ClNO$	229.0230	229.0296	-1.7	10.0
m/z 174	$C_7H_7Cl_2N$	174.9961	174.9916	-25.7	4
$[M-H]^-$			**TPMCF340c**		
m/z 338	$C_{14}H_9Cl_2N_2O_4$	338.9945	338.9943	-0.6	10.5
m/z 295	$C_{13}H_9Cl_2N_2O_2$	295.0047	295.0048	0.3	9.5
m/z 259	$C_{13}H_8ClN_2O_2$	259.0280	259.0280	0.0	10.5
m/z 229	$C_{13}H_8ClNO$	229.0300	229.0295	-2.2	10.5
m/z 174	$C_7H_7Cl_2N$	174.9961	174.9916	-25.7	4

(c)

Ion	Elemental composition	Exact mass [*m/z*]	Accurate mass [*m/z*]	Error [ppm]	DBE
$[M-H]^-$			**FFN**		
m/z 280	$C_{14}H_9F_3NO_2$	280.0591	280.0585	-2.1	9.5
m/z 236	$C_{13}H_9F_3N$	236.0693	236.0682	-4.7	8.5
m/z 216	$C_{13}H_8F_2N$	216.0630	216.0617	-6.0	9.5
m/z 196	$C_{13}H_7FN$	196.0568	196.0558	-5.1	10.5
$[M-H]^-$			**TPFFN310**		
m/z 309	$C_{14}H_8F_3N_2O_3$	309.0493	309.0493	0.0	10.5
m/z 279	$C_{14}H_8F_3NO_2$	279.0513	279.0512	-0.4	10.0
m/z 234	$C_{13}H_7F_3N$	234.0536	234.0531	-2.1	9.5
$[M-H]^-$			**TPFFN326a**		
m/z 325	$C_{14}H_8F_3N_2O_4$	325.0442	325.0439	-0.9	10.5
m/z 281	$C_{13}H_8F_3N_2O_2$	281.0543	281.0545	0.7	9.5
m/z 263	$C_{13}H_6F_3N_2O$	263.0438	263.0439	0.4	10.5
m/z 250	$C_{13}H_7F_3NO$	250.0485	250.0483	-0.8	9.5
$[M-H]^-$			**TPFFN326b**		

m/z 325	$C_{14}H_8F_3N_2O_4$	325.0442	325.0440	-0.6	10.5
m/z 281	$C_{13}H_8F_3N_2O_2$	281.0543	281.0542	-0.4	9.5
m/z 263	$C_{13}H_6F_3N_2O$	263.0438	263.0437	-0.4	10.5
m/z 251	$C_{13}H_8F_3NO$	251.0563	251.0561	-0.8	9
m/z 250	$C_{13}H_7F_3NO$	250.0485	250.0483	-0.8	9.5
m/z 230	$C_{13}H_6F_2NO$	230.0423	230.0418	-2.2	10.5
$[M-H]^-$		**TPFFN326c**			
m/z 325	$C_{14}H_8F_3N_2O_4$	325.0442	325.0440	-0.6	10.5
m/z 281	$C_{13}H_8F_3N_2O_2$	281.0543	281.0545	0.7	9.5
m/z 251	$C_{13}H_8F_3NO$	251.0563	251.0562	-0.4	9

(d)

Ion	Elemental composition	Exact mass [*m/z*]	Accurate mass [*m/z*]	Error [ppm]	DBE
$[M-H]^-$		**TFM**			
m/z 260	$C_{14}H_{11}ClNO_2$	260.0484	260.0486	0.8	9.5
m/z 216	$C_{13}H_{11}ClN$	216.0586	216.0580	-2.8	8.5
$[M-H]^-$		**TPTFM290**			
m/z 289	$C_{14}H_{10}ClN_2O_3$	289.0376	289.0387	1.8	10.5
m/z 258	$C_{14}H_9ClNO_2$	258.0316	258.0328	3.7	10.5
m/z 214	$C_{13}H_9ClN$	214.0418	214.0425	-4.4	9.5
$[M-H]^-$		**TPTFM306a**			
m/z 305	$C_{14}H_{10}ClN_2O_4$	305.0335	305.0333	-0.7	10.5
m/z 261	$C_{13}H_{10}ClN_2O_2$	261.0436	261.0434	-0.8	9.5
m/z 243	$C_{13}H_8ClN_2O$	243.0331	243.0326	-2.1	10.5
m/z 230	$C_{13}H_9ClNO$	230.0378	230.0373	-2.2	9.5
$[M-H]^-$		**TPTFM306b**			
m/z 305	$C_{14}H_{10}ClN_2O_4$	305.0335	305.0333	-0.7	10.5
m/z 261	$C_{13}H_{10}ClN_2O_2$	261.0436	261.0434	-0.8	9.5
m/z 243	$C_{13}H_8ClN_2O$	243.0320	243.0328	-1.2	10.5
m/z 230	$C_{13}H_9ClNO$	230.0367	230.0379	1.8	9.5
$[M-H]^-$		**TPTFM306c**			
m/z 305	$C_{14}H_{10}ClN_2O_4$	305.0335	305.0333	-0.7	10.5
m/z 261	$C_{13}H_{10}ClN_2O_2$	261.0436	261.0439	1.1	9.5

(e)

Ion	Elemental composition	Exact mass [*m/z*]	Accurate mass [*m/z*]	Mass Error [ppm]	DBE
$[M-H]^-$			**MFN**		
m/z 240	$C_{15}H_{14}NO_2$	240.1030	240.1026	-1.4	9.5
m/z 196	$C_{14}H_{14}N$	196.1132	196.1126	-2.8	8.5
$[M-H]^-$			**TPMFN270**		
m/z 269	$C_{15}H13N_2O_3$	269.0932	269.0932	0.0	10.5
m/z 238	$C_{15}H_{12}NO_2$	238.0874	238.0872	-0.5	10.5
m/z 194	$C_{14}H_{12}N$	194.0975	194.0969	-3.2	9.5
$[M-H]^-$			**TPMFN286a**		
m/z 285	$C_{15}H_{13}N_2O_4$	285.08808	285.0882	-3.2	10.5
m/z 241	$C_{14}H_{13}N_2O_2$	241.09825	241.0979	-1.3	9.5
m/z 223	$C_{14}H_{11}N_2O$	223.08769	223.0873	1.9	10.5
$[M-H]^-$			**TPMFN286b**		
m/z 285	$C_{15}H_{13}N_2O_4$	285.08808	285.0882	0.4	10.5
m/z 241	$C_{14}H_{13}N_2O_2$	241.09825	241.0980	-0.9	9.5
m/z 211	$C_{14}H_{13}NO$	211.10026	211.0997	-2.5	9.0
$[M-H]^-$			**TPMFN286c**		
m/z 285	$C_{15}H_{13}N_2O_4$	285.08808	285.0882	0.4	10.5
m/z 241	$C_{14}H_{13}N_2O_2$	241.09825	241.0981	-0.6	9.5
m/z 211	$C_{14}H_{13}NO$	211.10026	211.0995	-3.6	9.0

A detailed description of fragmentation pathways observed for parent drugs and the diverse TPs identified is provided hereinafter.

DCF and TPs. Compounds TPDCF324 and TPDCF340 eluting at 3.9 and 4.5 min, respectively, were described in detail in previous studies of our group [1,2].

Figure A-3. Full scan and MS^2 spectra acquired by HRMS in (-)-ESI mode of parent DCF and nitroso and nitro-TPs detected in samples collected from nitrifying activated sludge bioreactors after 36 days of experiment.

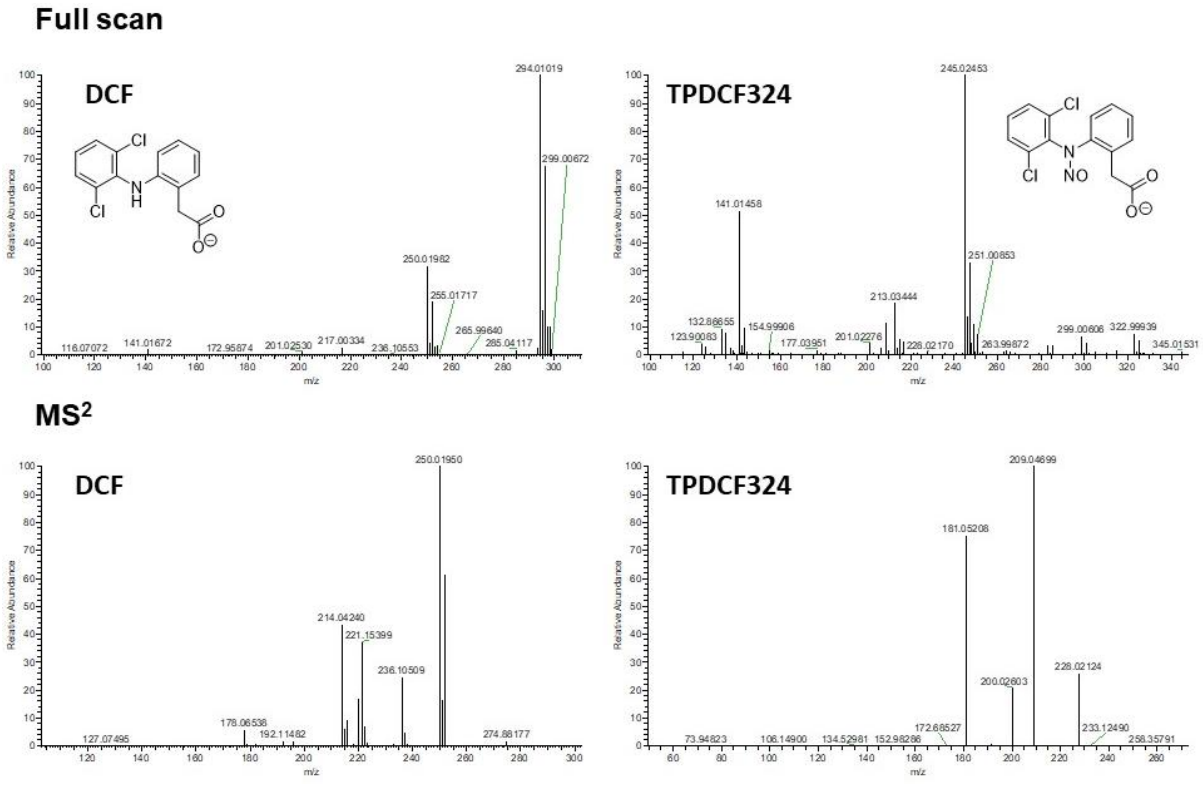

61

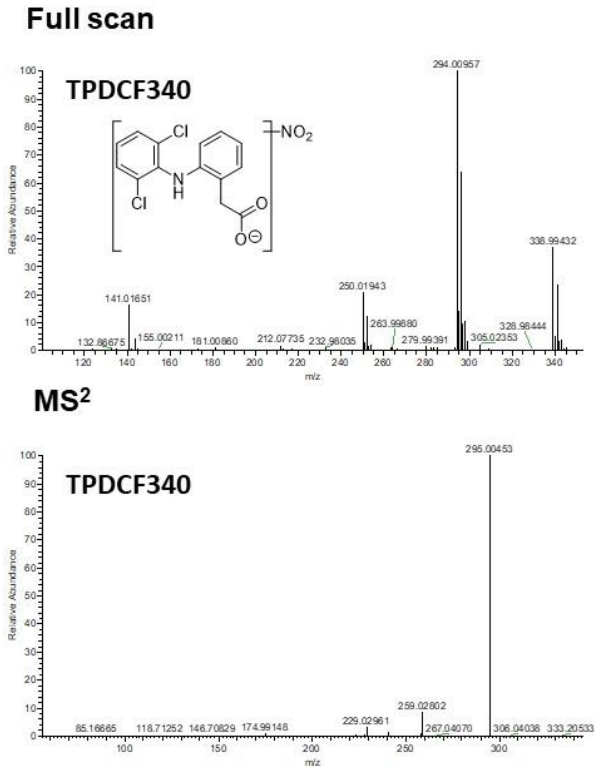

62

63 ***MCF and TPs.*** Parent compound MCF (eluting at 4.9 min) and its tentatively
64 identified derivatives TPMCF324 (at 3.8 min) and two isomers of TP340 a and c (at 4.6 and
65 5 min) were detected in microcosms amended with MCF (Figure 3). These TPs, which were

indeed isomers of TP324 and TP340, were tentatively attributed to originate from nitrosation and nitration of MCF molecule, as described previously for TPs of DCF (Table A-1b and Figure A-4). The (-)-ESI-MS^2 spectrum of the $[M-H]^-$ molecular ion of parent compound MCF at *m/z* 294.0095, and molecular formula $C_{14}H_{10}Cl_2NO_2$, shows the sequential loss of a -CO_2 molecule (44 Da) giving the fragment ion at *m/z* 250.0190, followed by the successive elimination of two molecules of -HCl (36 Da) producing two ions at *m/z* 214.0421 and 178.0652. MS^n experiments of *m/z* 250 confirmed further fragmentation to ion *m/z* 214. Eventually, ion at *m/z* 178 was corroborated as a fragment of *m/z* 214. Interestingly, (-)-ESI-MS full scan spectra of proposed TPMCF324 showed its corresponding $[M-H]^-$ molecular ion at *m/z* 322.9995 at a high relative abundance. Apparently, the differences in structural composition of TPMCF324 compared to its isomer TPDCF324, both with the same molecular composition $C_{14}H_9Cl_2N_2O_3$, reduced the lability of the N-NO or O-NO bond in the molecule. The product ion profile of the deprotonated molecule derived from the concurrent loss of -Cl• and -NO• (65 Da) giving the ion at *m/z* 258.0323. Further, a pseudo-MS^3 experiment selecting ion m/z 258 revealed a loss of -CO_2 to produce fragment ion at *m/z* 214.0421. Also diverse from DCF, two isomers of TPMCF340 were observed in MCF microcosms. The first isomer eluted, TPMCF340a was less abundant than the less polar TPMCF340c (Figure 3). Both compounds followed the same fragmentation pattern initiated with the decarboxylation of the $[M-H]^-$ molecular ions $C_{14}H_9Cl_2N_2O_4$ at *m/z* 338.9942 and 338.9943 to afford the respective fragment ions at *m/z* 295.0047 and 295.00479, followed by elimination of -HCl producing the corresponding anions at *m/z* 259.02863 and 295.0048; and eventual cleavage of -NO• (30 Da) giving the fragments at *m/z* 229.0296 and 229.0295, respectively. The fragmentation pathway of both isomers of TPMCF340 was similar to that described previously for TPDCF340 [1]. However, the diagnostic ion evidencing the release of -NO_2 from the molecule was not observed in either isomer of TPMCF340 as it was noticed before for TPDCF340.

Figure A-4. Full scan and MS^2 spectra acquired by HRMS in (-)-ESI mode of parent MCF and nitroso and nitro-TPs detected in samples collected from nitrifying activated sludge bioreactors after 36 days of experiment.

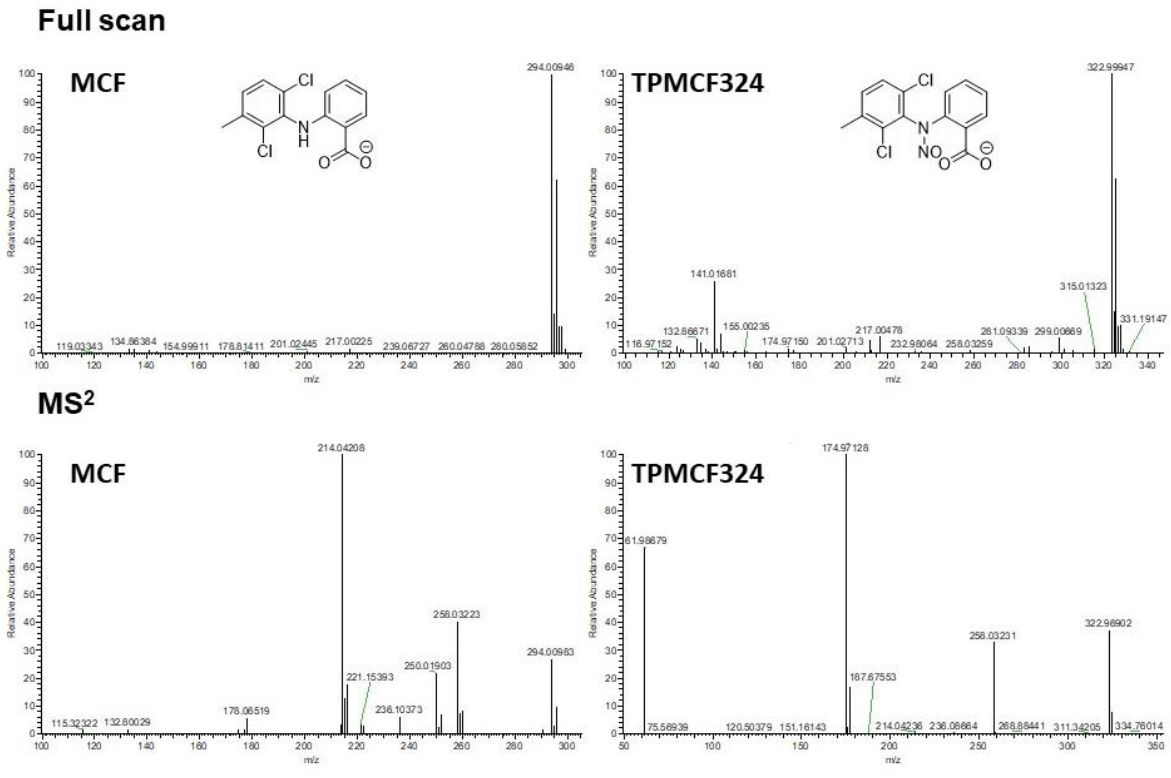

95

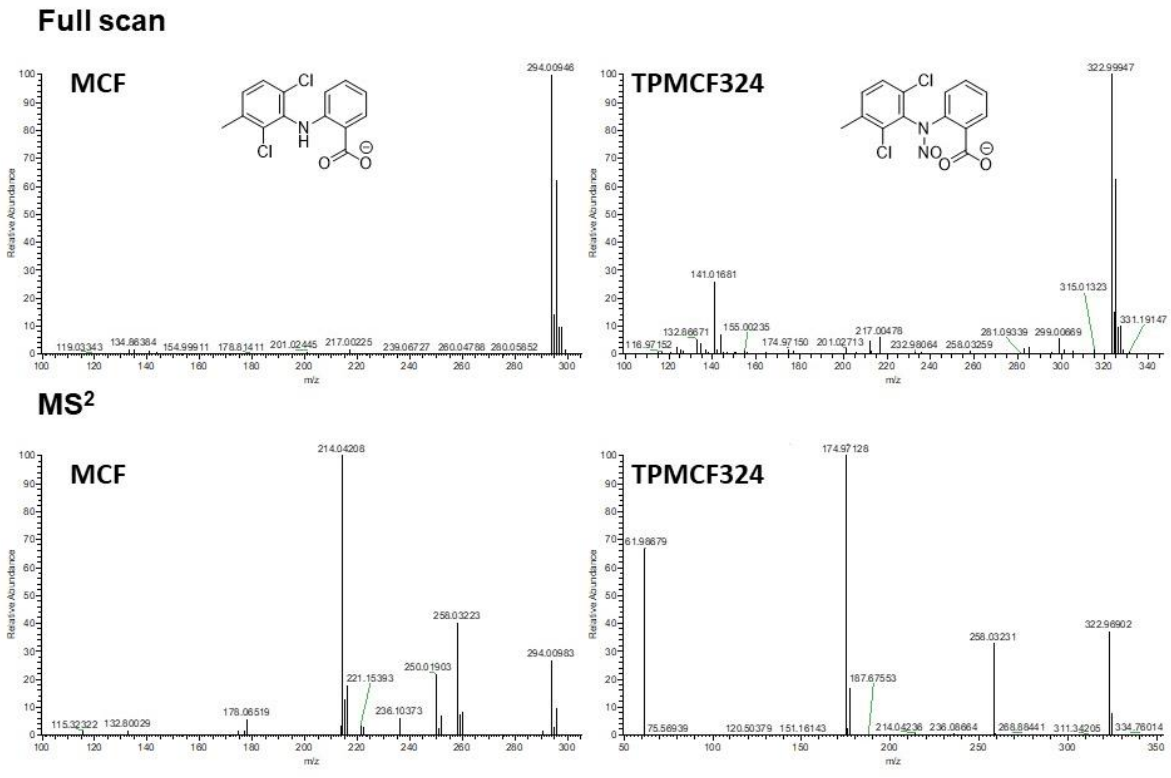

96

97 ***FFN and TPs.*** Analysis of samples collected from FFN bioreactors evidenced the
98 presence of a compound eluting at 4.2 min, TPFFN310, which was conjectured to be the
99 nitrosation product of FFN (eluting at 4.8 min) (Figure 3). Three additional peaks were
100 observed at 4.6, 4.8 and 5 min of elution, which were tentatively attributed to different

isomers of nitration products of FFN, TPFFN326a, TPFFN326b and TPFFN326c, respectively. The (-)-ESI-MS^2 spectrum of FFN (Table A-1c and Figure A-5) shows a deprotonated molecule at *m/z* 280.0585 corresponding to the molecular formula $C_{14}H_9F_3NO_2$. The loss of -CO_2 resulted in the formation of a major fragment ion at *m/z* 236.0682. Further fragmentation was identified as the sequential loss of -HF molecules (20 Da) from the trifluorinated anion to afford the respective fragment ions at *m/z* 216.0617, and 196.0558. As observed previously for TPMCF324, the full scan spectra of TPFFN310 showed a molecular ion at *m/z* 309.0493 with a high relative abundance confirming the molecular composition $C_{14}H_8F_3N_2O_3$. Main fragment ions of TPFFN310 were already detected in full scan acquisition mode, which evidenced the lability of the molecule, as seen previously for TPDCF324. Interestingly, the product ion profile of TPFFN310 showed the initial elimination of $NO^{\cdot}$ generating a fragment ion at *m/z* 279.0512. The fragmentation pattern observed afterwards was similar to that recorded for the parent drug FFN following a decarboxylation of the molecule and affording the fragment ion at *m/z* 234.0531. According to full scan and MS^2 spectra acquired for the three isomers of TPFFN326 with molecular formula $C_{14}H_8F_3N_2O_4$, differences in relative abundances of molecular ions and major fragment ions were observed. Relative abundance of molecular ion of TPFFN326 b was substantially lower than the others corresponding to TPFFN326a and TPFFN326c. The MS^2 spectra of the $[M-H]^-$ molecular ion of TPFFN326a *m/z* 325.0439 showed three major fragmentation ions at *m/z* 281.0545, 263.0439 and 250.0483. According to the proposed elemental composition and mass errors recorded, these fragments were assigned to the initial decarboxylation of the deprotonated molecule, followed by the elimination of -H_2O or -HNO. However, pseudo-MS^3 experiments selecting ion *m/z* 281 could not confirm fragment ions at *m/z* 263 and 250 as its products, since no further fragmentation was observed. Therefore, the identification of fragment ions deriving from the anion at *m/z* 281 was merely conjectured. The fragmentation patterns of molecular ions at *m/z* 325.0440 and 325.0440 corresponding to TPFFN326b and TPFFN326c were similar, with respective major fragment ions at *m/z* 281.0542 and 251.0561; and at *m/z* 281.0545 and 251.0562, corresponding to the elimination of -CO_2 and -NO•. Additional fragment ions were observed at *m/z* 263.0439 and 263.0437 for TPFFN326a and TPFFN326b, respectively, which could be derived from the elimination of -H_2O from the fragment ion at *m/z* 281. Further fragmentation was observed for TPFFN326b with ion at *m/z* 230.0418. Pseudo-MS^3 experiments selecting ion *m/z* 250 confirmed the loss of a molecule of -HF to generate the fragment at *m/z* 230.

Figure A-5. Full scan and MS^2 spectra acquired by HRMS in (-)-ESI mode of parent FFN and nitroso and nitro-TPs detected in samples collected from nitrifying activated sludge bioreactors after 36 days of experiment.

Full scan

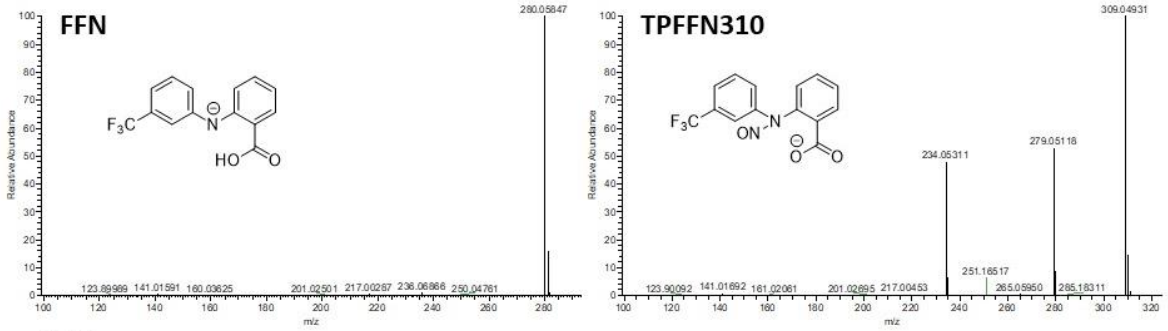

MS^2

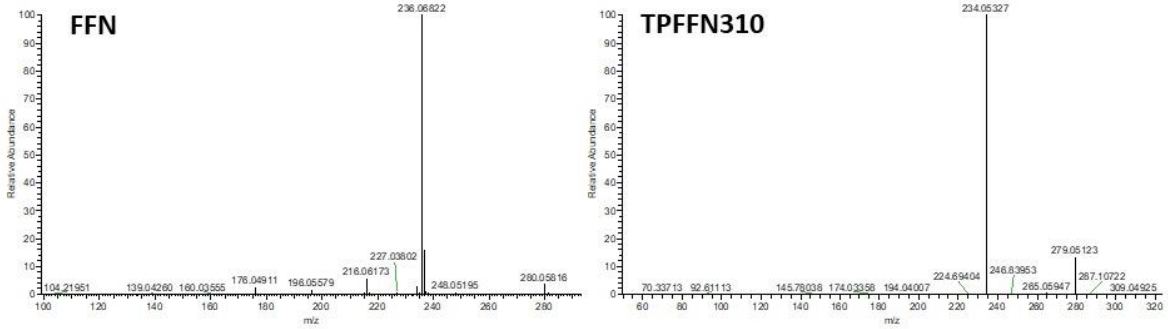

137

Full scan

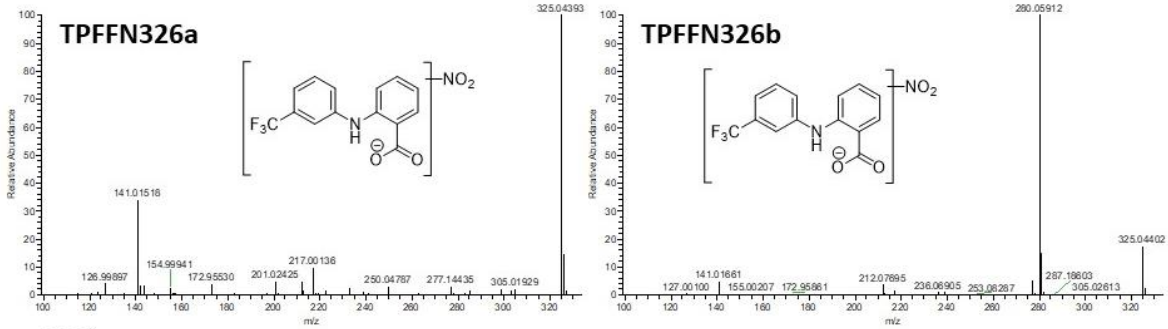

MS^2

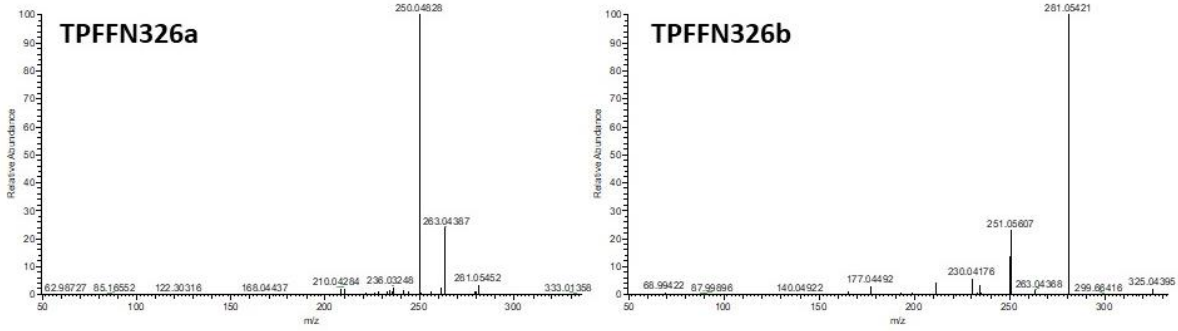

138

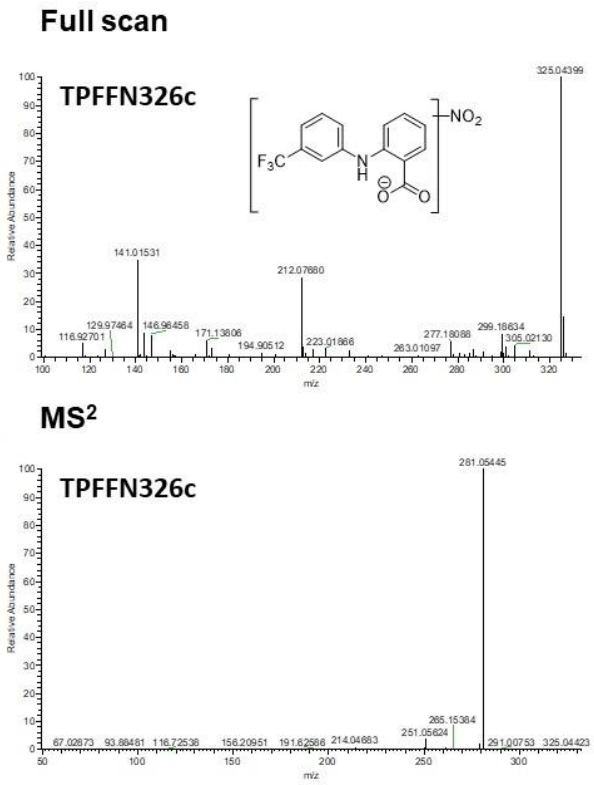

TFM and TPs. Chromatographic separation of analysed samples collected from TFM microcosms showed the parent drug eluting at 4.9 min, a compound identified as TPTFM290 at 4.0 min and 3 peaks eluting at 4.6, 4.7 and 5.0 min corresponding to three isomers of TPTFM306a, b and c (Figure 3). The structural elucidation of TPTFM290 and TPTFM306 tentatively assigned the compounds as the respective products of nitrosation and nitration of TFM. The (-)-ESI-MS full scan spectrum of TFM (Table A-1d and Figure A-6) showed a deprotonated molecule at *m/z* 260.0486 corroborating the molecular formula $C_{14}H_{11}ClNO_2$. According to the (-)-ESI-MS^2 spectrum of TFM, the major fragment ion observed at *m/z* 216.0580 could be identified as a decarboxylation product of the $[M-H]^-$ molecular ion. As regards proposed TPTFM290, recorded full scan spectrum of TFM bioreactors aliquots confirmed the elemental composition $C_{14}H_{10}ClN_2O_3$ of the $[M-H]^-$ molecular ion at *m/z* 289.0387. Pseudo-MS^3 experiments selecting the molecular ion at *m/z* 289 produced the major fragment ions at *m/z* 258.0328 and 214.0425 which were assigned to the sequential loss of -HNO and -CO_2 molecules. Additional pseudo-MS^3 experiments confirmed ion at m/z 214 as a fragment of ion at *m/z* 258. The full scan spectrum acquired also confirmed the three isomers (a, b and c) of TPTFM306 showing respective deprotonated molecules at *m/z* 305.0333, with elemental composition $C_{14}H_{10}ClN_2O_4$. Pseudo-MS^3 experiments allowed assigning the major fragment ion for TPTFM306a, TPTFM306b and TPTFM306c at respective *m/z* 261.0434, 261.0434 and 261.0439 as the decarboxylation product of the deprotonated molecular ion. Although this main fragment ion was observed in the three (-)-

ESI-MS^2 spectra acquired for each isomer, the complexity of fragmentation profiles differed among isomers. For isomer c no additional fragments were observed. Fragmentation patterns for TPTFM306a and TPTFM306b were similar, showing fragment ions at *m/z* 243.0326 and 243.0328 corresponding to the loss of -H_2O from the molecule at m/z 261; and *m/z* 230.0373 and 230.0379 as a product of the elimination of -HNO from the same ion. However, pseudo-MS^3 experiments could not confirm the sequential fragmentation of TPTFM306b, while for TPTFM306a only fragment at m/z 230 was confirmed as a product of major fragment ion at *m/z* 261.

Figure A-6. Full scan and MS^2 spectra acquired by HRMS in (-)-ESI mode of parent TFM and nitroso and nitro-TPs detected in samples collected from nitrifying activated sludge bioreactors after 36 days of experiment.

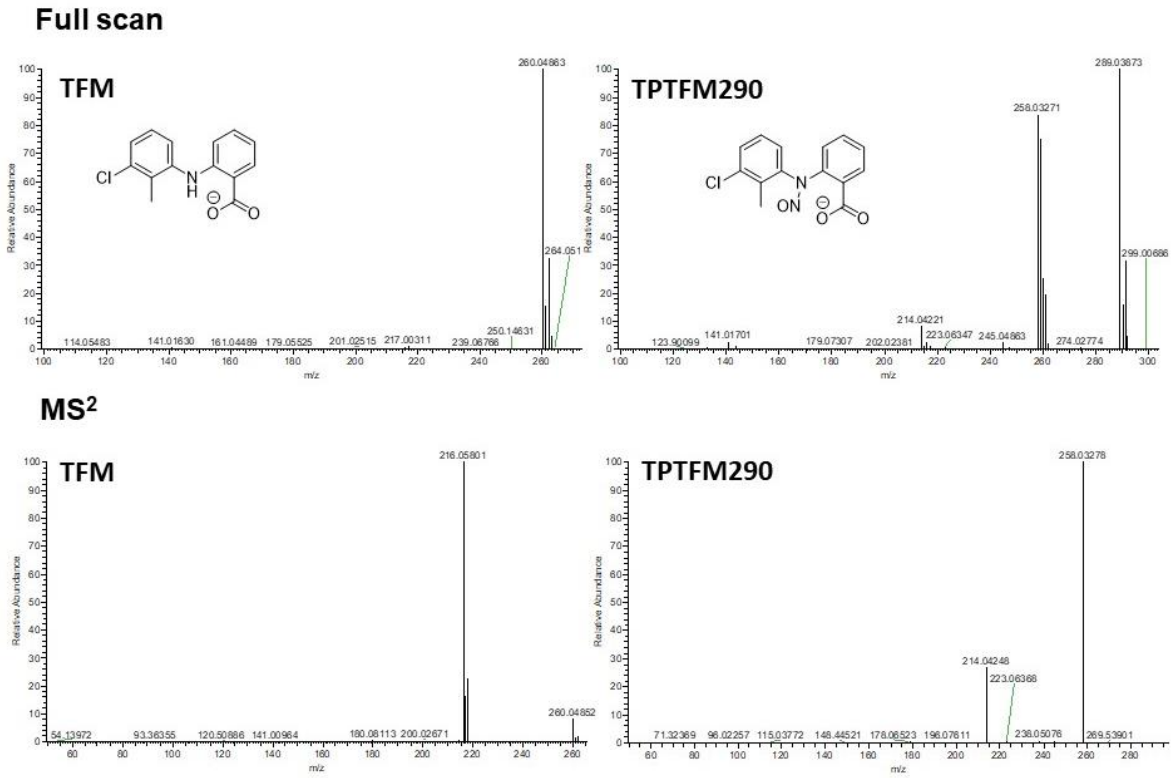

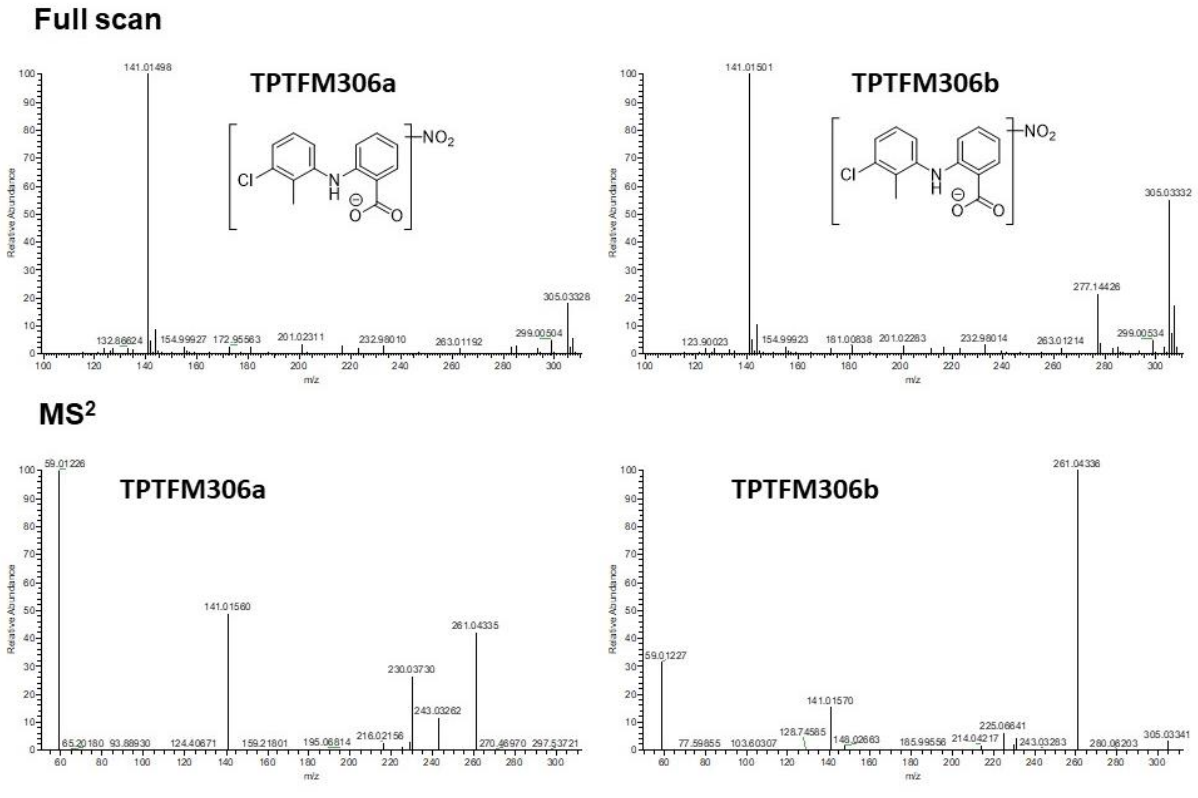

172

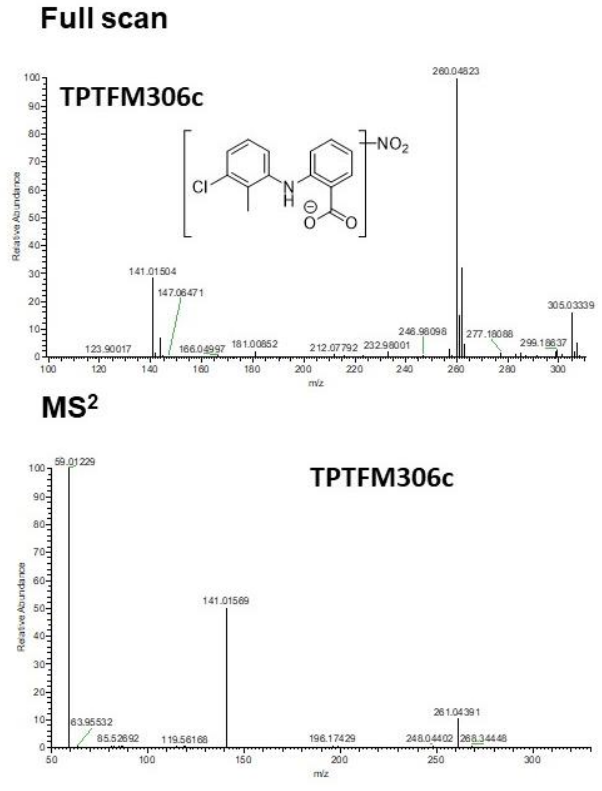

173

174 ***MFN and TPs.*** Parent drug MFN and its proposed derivatives TPMFN270 and three
175 isomers of TPMFN286a, b and c were detected in bioreactors spiked with MFN at respective
176 elution times 4.8, 3.8, 4.4, 4.6 and 4.8 min (Figure 3). According to the (-)-ESI-MS full scan,

MS^2 and pseudo-MS^3 experiments acquired for these compounds, TPMFN270 and TPMFN286 isomers were tentatively identified as the corresponding derivatives of the nitrosation and nitration of MFN under bioreactors conditions. The product ion profile of the deprotonated molecule of MFN (Table A-1e and Figure A-7), with confirmed elemental composition $C_{15}H_{14}NO_2$ and at *m/z* 240.1026, showed a major fragment ion at *m/z* 196.1126 which corresponded to the decarboxylation of the molecular ion. Regarding TPMFN270, its corresponding $[M-H]^-$ molecular ion at m/z 269.0932 observed in the full scan spectrum affirmed the chemical formula $C_{15}H_{13}N_2O_3$. Pseudo-MS^3 experiments selecting ion at m/z 269, and subsequent ions observed, allowed to describe the fragmentation pattern of this derivative. This started with the elimination of -HNO from the deprotonated molecule to generate a major fragment ion at *m/z* 238.0872, followed by the loss of $-CO_2$ affording the secondary fragment ion at *m/z* 194.0969. The full scan spectrum of the depronated molecules of TPMFN286a, TPMFN286b and TPMFN286c at *m/z* 285.0882, corroborated their elemental composition $C_{15}H_{13}N_2O_4$. Their MS^2 spectrums showed major fragment ions at *m/z* 241.0979, 241.0980 and 241.0981, for respective TPMFN286a, TPMFN286b and TPMFN286c, which were identified as the product of decarboxylation of molecular ion. An additional fragment, with low relative intensity, was observed at *m/z* 223.0873, for TPMFN286a, which was conjectured as the product of the loss of $-H_2O$ from fragment at *m/z* 241. Eventual pseudo-MS^3 experiments selecting fragment ion at *m/z* 241 evidenced further fragmentation to afford respective fragment ions of TPMFN286b and TPMFN286c at *m/z* 211.0997 and 211.0995 assigned to the loss of -NO•.

Figure A-7. Full scan and MS^2 spectra acquired by HRMS in (-)-ESI mode of parent MFN and nitroso and nitro-TPs detected in samples collected from activated sludge bioreactors after 36 days of experiment.

Full scan

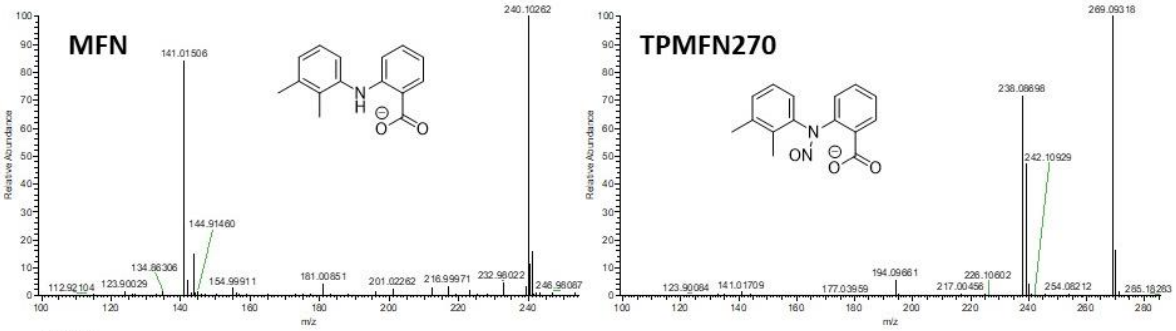

MS²

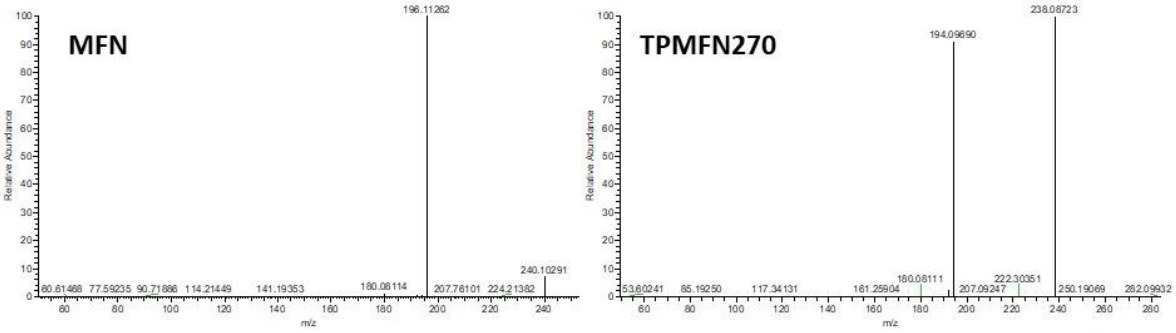

201

Full scan

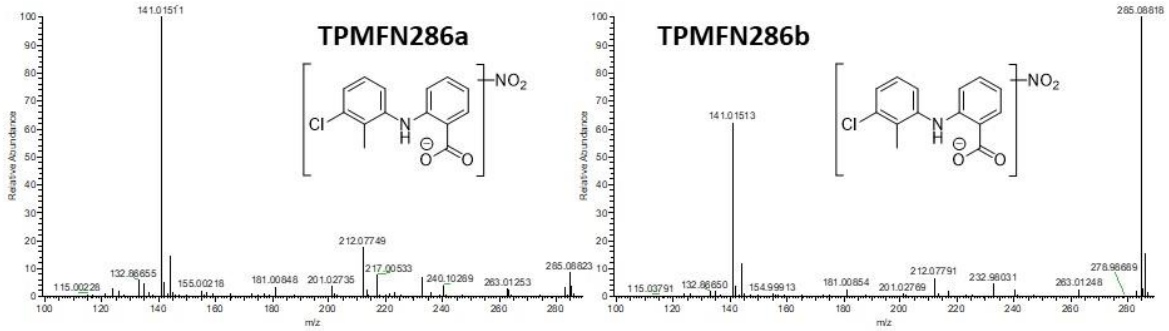

MS²

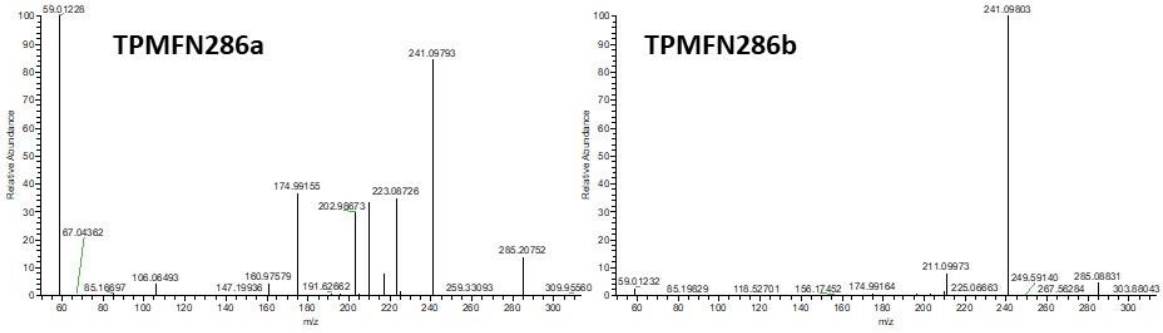

202

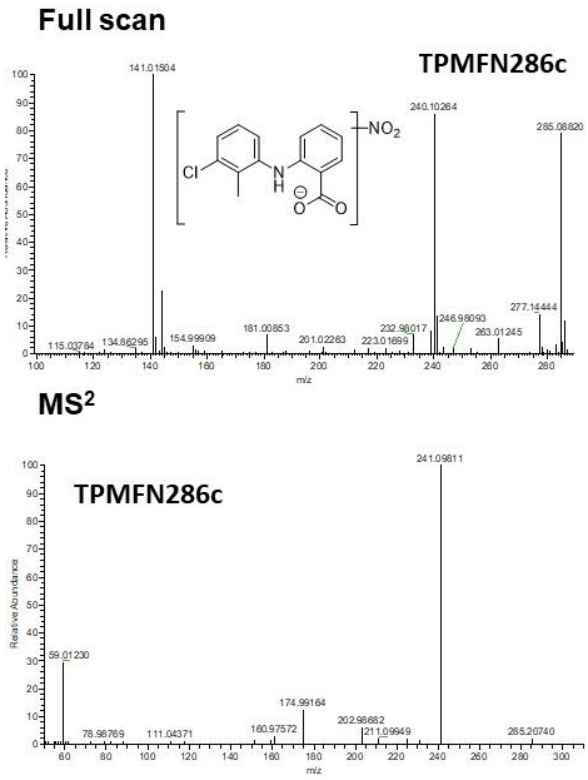

203

204

205 **3.3.2. Mechanisms of biotransformation and biodegradability of DCF and related**
206 **NSAIDs in the different nitrifying activated sludge batch reactors**

207 **Figure A-8.** Qualitative biotransformation profiles of DCF and its biotransformation products
208 TPDCF324 and TPDCF340 in biodegradation experiments in nitrifying activated sludge: **(a)**
209 batch-reactor R2, with AOB inhibition (ATU addition), **(b)** batch-reactor R3, with ammonia-
210 oxidizing microorganisms s (AOB and AOA) and NOB inhibition (SA addition), and **(c)** batch-
211 reactor R4, absence of NH_3. Qualitative evolution of levels of parent compound and TP are
212 represented as A/A_0 (%) (Y-axis) plotted against time course in hours of the biodegradation
213 experiment (X-axis). Y-axis indicates the peak areas of the extracted ion chromatograms of
214 DCF or its TPs (A) normalized to the initial peak area of DCF at maximum initial
215 concentration (A_0) calculated as percentages.

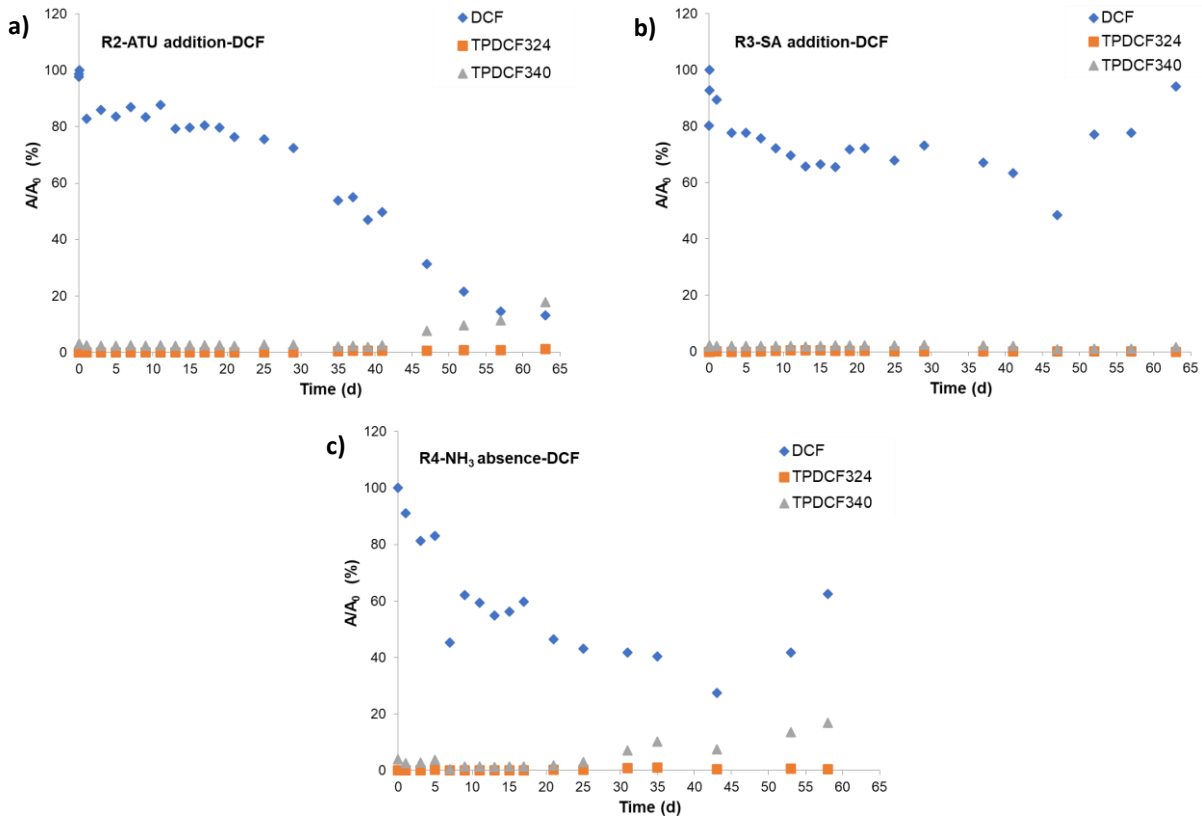

Figure A-9. Qualitative biotransformation profiles of MCF and its biotransformation products TP324M and TP340M in biodegradation experiments in NAS: **(a)** batch-reactor R2, with AOB inhibition (ATU addition), and **(b)** batch-reactor R3, with AOMs (AOB and AOA) and NOB inhibition (SA addition) Qualitative evolution of levels of parent compound and TP are represented as A/A_0 (%) (Y-axis) plotted against time course in hours of the biodegradation experiment (X-axis). Y-axis indicates the peak areas of the extracted ion chromatograms of MCF or its TPs (A) normalized to the initial peak area of MCF at maximum initial concentration (A_0) calculated as percentages.

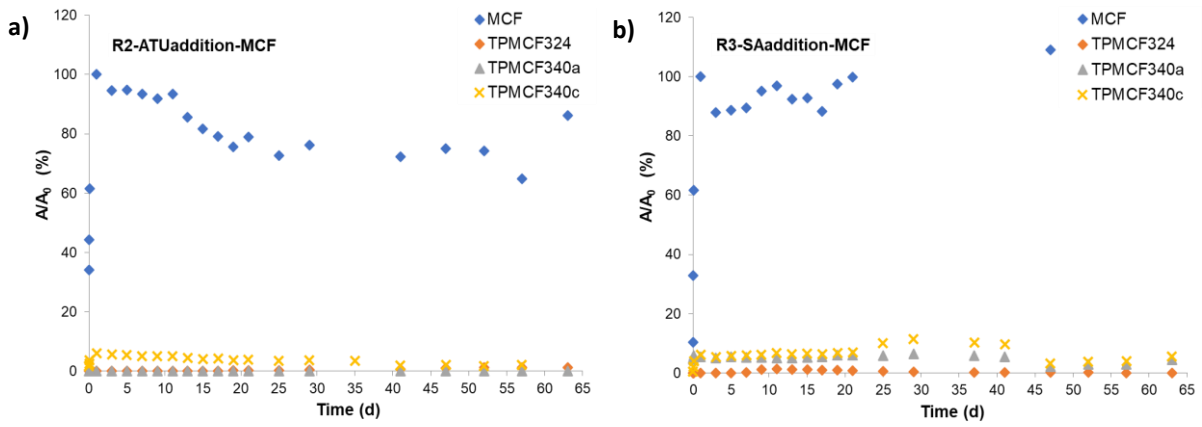

Figure A-10. Qualitative biotransformation profiles of FFN and its biotransformation products TPFFN310 and TPFFN326 in biodegradation experiments in NAS: **(a)** batch-reactor R2, with AOB inhibition (ATU addition), and **(b)** batch-reactor R3, with AOM (AOB and AOA) and NOB inhibition (SA addition). Qualitative evolution of levels of parent compound and TP are represented as A/A_0 (%) (Y-axis) plotted against time course in hours of the biodegradation experiment (X-axis). Y-axis indicates the peak areas of the extracted ion chromatograms of FFN or its TPs (A) normalized to the initial peak area of FFN at maximum initial concentration (A_0) calculated as percentages.

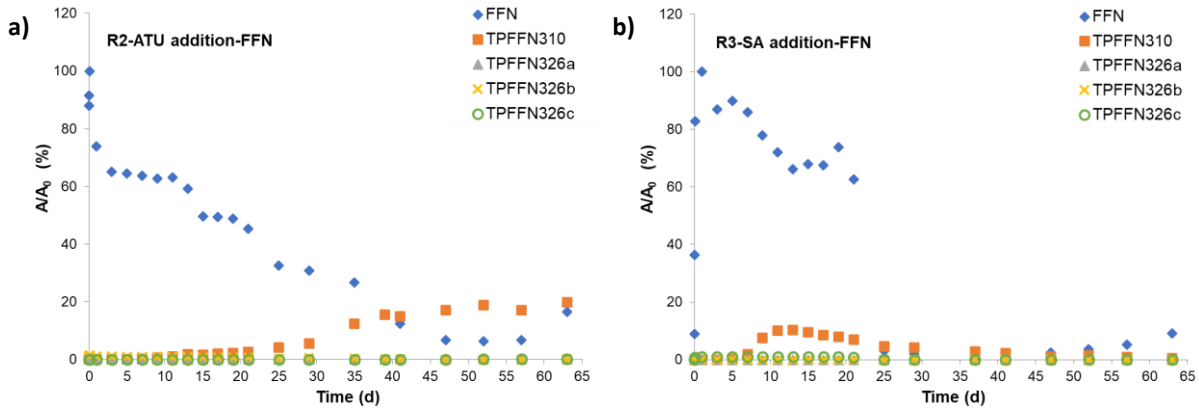

Figure A-11. Qualitative biotransformation profiles of TFM and its biotransformation products TPTFM290 and TPTFM306 in biodegradation experiments in NAS: **(a)** batch-reactor R2, with AOB inhibition (ATU addition), and **(b)** batch-reactor R3, with AOM (AOB and AOA) and NOB inhibition (SA addition). Qualitative evolution of levels of parent compound and TP are represented as A/A_0 (%) (Y-axis) plotted against time course in hours of the biodegradation experiment (X-axis). Y-axis indicates the peak areas of the extracted ion chromatograms of TFM or its TPs (A) normalized to the initial peak area of TFM at maximum initial concentration (A_0) calculated as percentages.

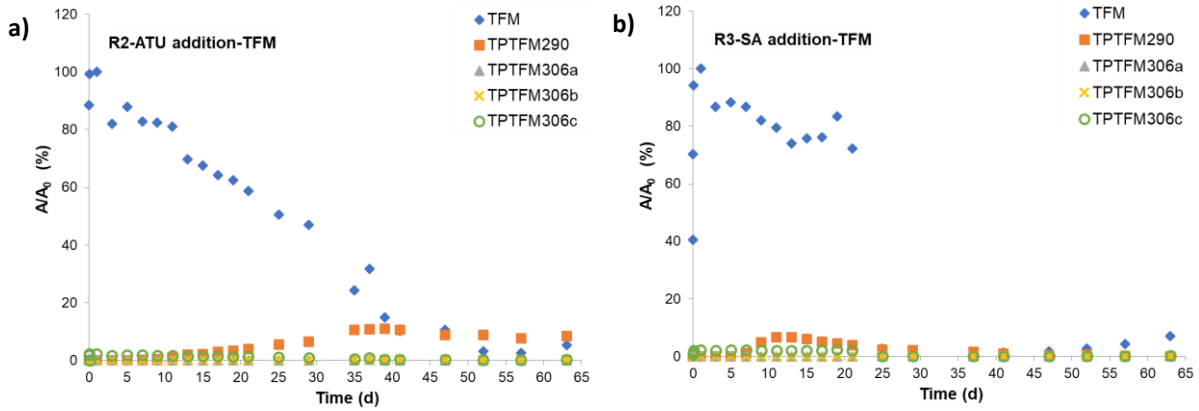

Figure A-12. Qualitative biotransformation profiles of MFN and its biotransformation products TPMFN270 and TPMFN286 in biodegradation experiments in NAS: **(a)** batch-reactor R2, with AOB inhibition (ATU addition), and **(b)** batch-reactor R3, with AOMs (AOB and AOA) and NOB inhibition (SA addition). Qualitative evolution of levels of parent compound and TP are represented as A/A_0 (%) (Y-axis) plotted against time course in hours of the biodegradation experiment (X-axis). Y-axis indicates the peak areas of the extracted ion chromatograms of MFN or its TPs (A) normalized to the initial peak area of MFN at maximum initial concentration (A_0) calculated as percentages.

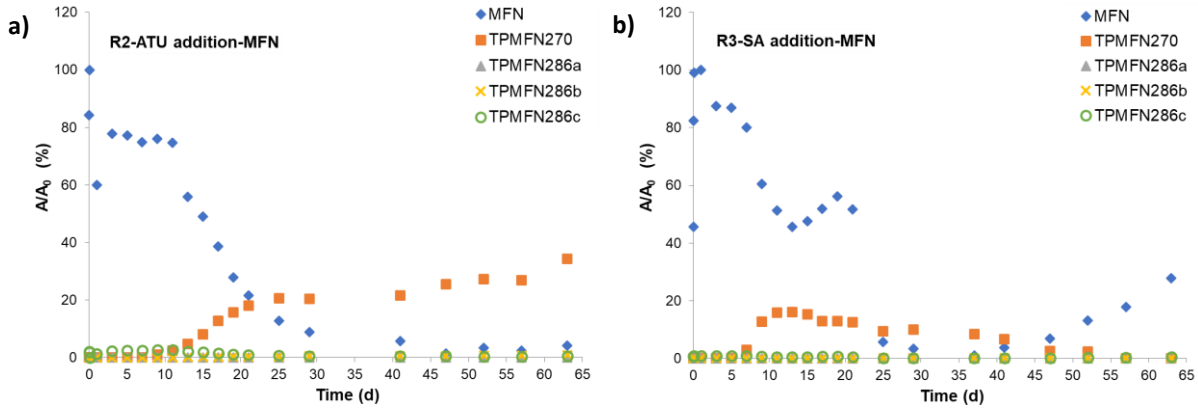

Bacteria cell viability. Live and dead bacteria were measured at the end of the long-term biotransformation experiment (Figure A-22). Overall, the maximum number of live cells measured was ~5×10^8 in R2 spiked with DCF, while the minimum determined was ~2×10^8 in R2 fortified with all NSAIDs (Figure A-23a). Regarding dead bacteria, ~8.5×10^8 cells in R3 were the maximum measured, while the minimum of ~2.5×10^8 cells was determined in R1 spiked with DCF (Figure A-23b). The quantity of live cells was higher in R2 respective to R1 batch-reactors individually spiked with DCF, MCF, FFN; whereas the opposite trend was observed in microcosms spiked with TFM and MFN. As a matter of fact, trends for dead cells were the contrary, being more numerous in R2 microcosms fortified with TFM and MFN compared to R1; while dead cells were less in R1 spiked with DCF, MCF and FFN compared to R2. Live/dead bacteria ratios (L/D) (Table A-2) calculated in batch-reactors R1, R2 and R4 amended with DCF had similar values over 1, meaning that the number of live bacteria under the different conditions held in the microcosms was almost even (Figure A-23). Only in the case of batch-reactors spiked with MCF, a considerably higher number of dead bacteria was measured in R1 compared to R2, with a L/D in R1 that was half the ratio calculated in R2; in which live cells were a little more numerous than dead ones. Similar to DCF, L/D in batch-reactors R1 and R2 fortified with FFN were at the same level, where dead bacteria

cells counted slightly higher than live cells. Microcosms R1 and R2 fortified with TFM showed marked differences in L/D, while the quantity of live cells in R1 was noticeable compared to dead cells; the contrary was observed in R2 with more numerous dead cells measured relative to live ones. As it was observed for FFN batch-reactors, the number of dead cells measured in R1 and R2 spiked with MFN was higher than live cells. However, L/D was substantially lower in R2 compared to R1, meaning that the quantity of dead cells was higher in R2 compared to R1. L/D measured in batch-reactor R3 spiked with all test compounds was the lowest, meaning that the number of live cells was scarce compared to dead bacteria.

Figure A-13. Bacteria observed during live/dead (green/red) assay for the determination of live/dead bacteria ratio in the activated sludge of the different microcosms investigated (a) shows bioreactors R1, R2 and R4 spiked with DCF while R3 was spiked with a mixture of all NSAIDs tested (i.e. DCF, MFN, FFN, MCF and TFM); and (b) displays bioreactors R1 and R3 spiked with MCF and TFM.

(a)

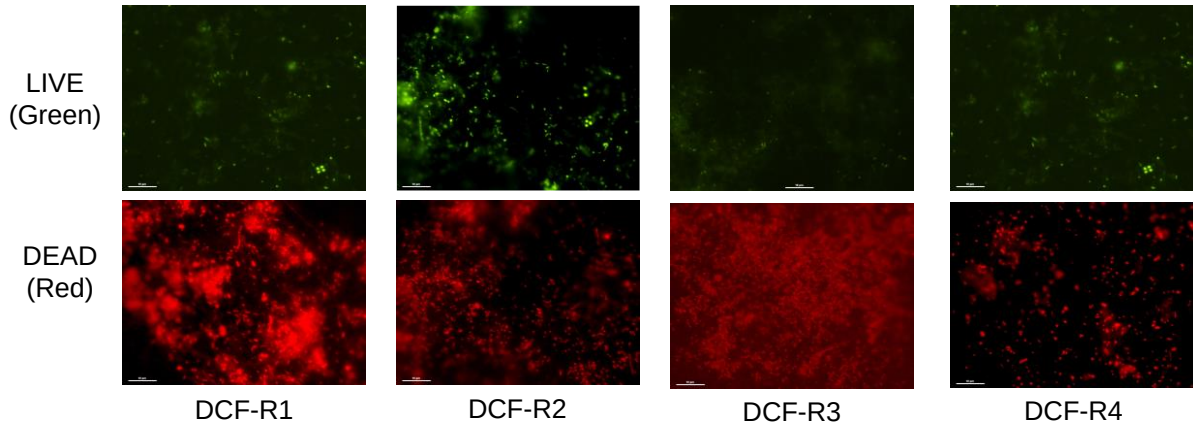

(b)

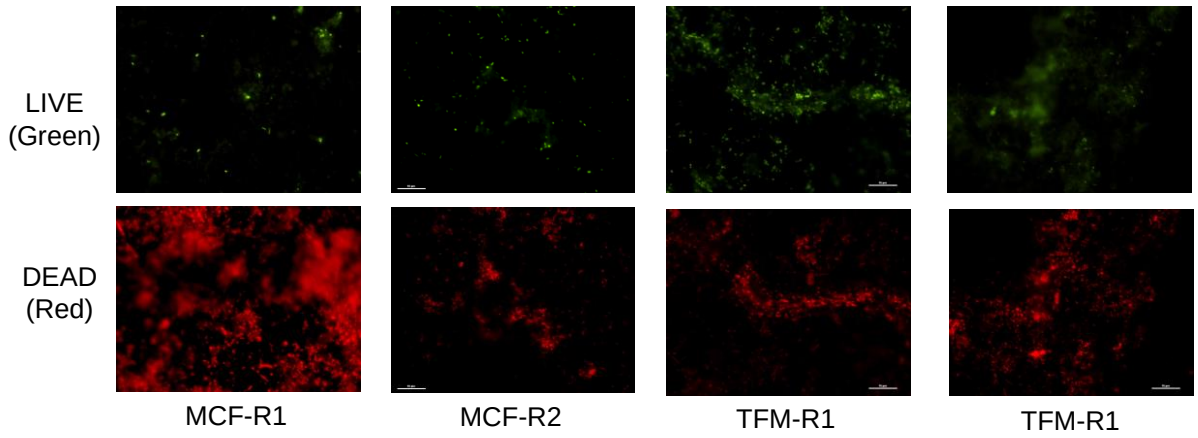

289

290 **Figure A-14. (a)** Live and **(b)** dead bacteria cells measured in activated sludge collected
291 from each bioreactor investigated i.e. R1 and R2 amended with individual NSAIDs studied;
292 while R3 amended with a mixture of all selected NSAIDs; and R4 only spiked with DCF.
293 Twenty random fields were chosen and observed, and the amount of live and dead cells in
294 activated sludge was calculated by counting green/red cells in 20 random fields per sample.
295 **(a)**

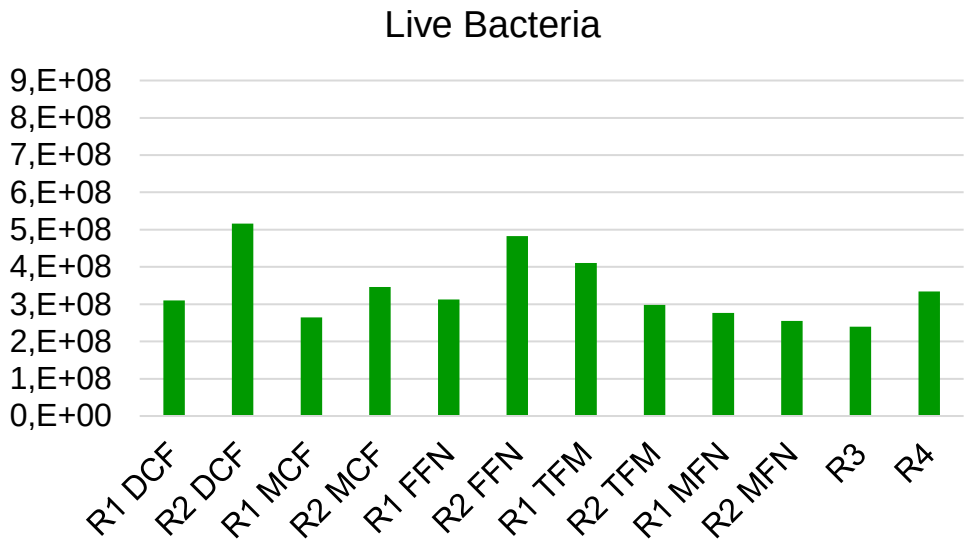

296

297 **(b)**

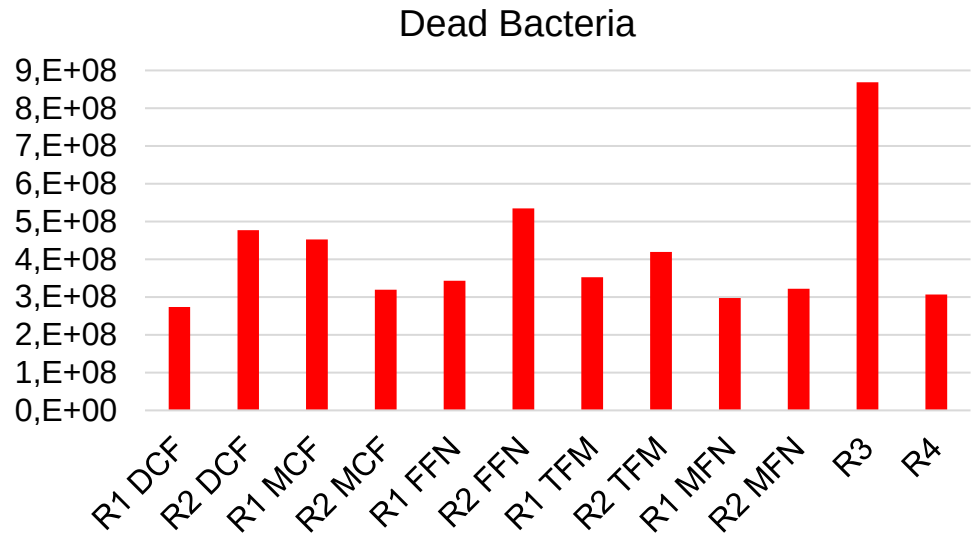

Table A-2. Live/Dead bacteria cells ratio in activated sludge collected from each bioreactor investigated i.e. R1 and R2 amended with individual NSAIDs studied; while R3 amended with a mixture of all selected NSAIDs; and R4 only spiked with DCF. Twenty random fields were chosen and observed, and the amount of live and dead cells in activated sludge was calculated by counting green/red cells in 20 random fields per sample.

Compound	Live/Dead bacteria ratio			
	R1	R2	R3	R4
DCF	1,13	1,08		1,09
MCF	0,58	1,09		
FFN	0,91	0,90		
TFM	1,16	0,71		
MFN	0,93	0,79		
ALL			0,28	

Total percentages of formation for nitroso and nitro-TPs of NSAIDs identified. Total levels of Nitrogen-derivatives of DCF, MCF, FFN, TFM and MFN were calculated according to maximum percentages of TPs triggered among the different microcosms R1-R3 shown in Table A-3. DCF nitroso and nitro-TPs were found to represent up to 19% of DCF initial concentration in batch reactor R2, followed by a total of 5% in R1 and 3% in R3. Nitrogen-derivatives of MCF summed up to 12% of MCF's spiked concentration in R3, while only 5% and 2% were generated in R1 and R2. A total of 29% of the initial concentration of FFN was biotransformed into its nitrogen-TPs in microcosms R1, while 21% and 12% were triggered in batch-reactors R2 and R3. TFM was also nitrosated and nitrated at the highest extent in R1, summing up to 15% of initial levels and up to 11% and 9% in R2 and R3.

315 Eventually, nitroso and nitro-TPs of MFN represented 34 and 33% of MFN initial
316 concentration in R2 and R1 microcosms, whereas 17% was the total percentage produced in
317 R3.

318 **Table A-3.** Maximum values of removal of NSAIDs investigated and formation of their
319 nitroso and nitro TPs in activated sludge from the three different batch degradation
320 experiments (i.e. R1, R2 and R3); t (d) indicates day of experiment when maximum removal
321 of NSAIDs investigated and maximum levels of TPs identified were observed. Removal
322 percentages were calculated as 100-A/A_0 (%) while percentage of TPs formation was
323 quantified as A/A_0 (%), where A is the peak area of the extracted ion chromatograms of the
324 compound and normalized to the initial peak area of NSAID at maximum initial concentration
325 (A_0) calculated as percentages.

NSAIDs investigated		R1		R2		R3		R4	
		Removal (%)	t (d)	Removal (%)	t (d)	Removal (%)	t (d)	Removal (%)	t (d)
Parent compound	DCF	56.7	39	86.9	63	51.6	47	72.5	43
	MCF	27.0	25	35.2	57	12.0	3	-	-
	FFN	93.4	57	93.6	52	99.3	37	-	-
	TFM	87.7	52	97.4	52	99.5	37	-	-
	MFN	98.1	57	98.7	47	99.0	37	-	-
		A/A_0 (%)	t (d)	A/A_0 (%)	t (d)	A/A_0 (%)	t (d)	A/A_0 (%)	t (d)
Nitroso-TPs	TPDCF324	0.6	37	1.2	63	0.5	13	1.0	35
	TPMCF324	4.0	57	1.7	37	1.3	11	-	-
	TPFFN310	28.1	63	19.8	63	10.3	13	-	-
	TPTFM290	14.4	52	11.0	39	6.7	11	-	-
	TPMFN270	30.8	63	34.3	63	16.1	13	-	-
Nitro-TPs	TPDCF340	4.1	41	17.8	63	2.5	29	16.9	58
	TPMCF340a	1.1	63	0.1	37	6.4	29	-	-
	TPMCF340c	6.3	3	6.1	1	11.4	29	-	-
	TPFFN326a	1.6	7	0.3	41	0.0	37	-	-
	TPFFN326b	1.8	5	1.4	<1	0.1	1	-	-
	TPFFN326c	0.7	63	0.1	63	1.1	19	-	-
	TPTFM306a	0.2	41	0.1	37	0.0	-	-	-
	TPTFM306b	0.9	63	0.5	37	0.0	-	-	-
	TPTFM306c	1.8	5	2.2	<1	2.3	19	-	-
	TPMFN286a	0.2	63	0.1	63	0.0	-	-	-
	TPMFN286b	2.9	63	0.9	63	0.2	57	-	-
	TPMFN286c	3.3	1	2.6	11	0.9	<1	-	-

326

In general, the nitrosation of MCF and DCF was minor compared to MFN, TFM and FFN. Indeed, formation percentages in all reactors were minor for TPMCF324 and TPDCF324 (max. of 1-4%), while TPMFN270 (max. of 16-34%) was the more abundant followed by TPFFN310 (max. 10-28%) and TPTFM290 (max. 7-14%). Overall, formation of these nitroso-TPs was triggered at higher levels in microcosms R1, followed by R2 and R3, where the percentages determined were substantially lower. Regarding nitro-derivatives, TP340 (max. 3-18%) was the major TP among the others in all microcosms (max. >1-11%), whose formation was triggered in a lesser extent being the nitro-TPs of MCF the more abundant on average (max. >1%-11%), followed by those for MFN (max. >1-3%), TFM and FFN (max. >1-2%). Overall, TPDCF340 and TPMCF340c were the major TPs detected at 18% and 11% in R2 and R3, respectively. The formation of the rest of nitro-TPs was triggered to a much lesser extent in all microcosms.

Table A-4. Spearman correlation coefficients Parent compound/Nitroso-TP; Parent compound/ nitro-TP. Correlation coefficients were calculated based on levels of parent compounds and TPs determined along 21 monitoring days of the biodegradation experiments performed in the different microcosms R1-R3. Given that biotransformation profiles for the majority of compounds did not follow a normal distribution, spearman coefficients (non-parametric) were calculated. Best correlations are highlighted in bold and cursive

Compound	R1				R2				R3			
DCF	TPDCF324	TPDCF340			TPDCF324	TPDCF340			TPDCF324	TPDCF340		
	-0.941**	-0.603**			-0.923**	-0.097			-0.777**	-0.091		
TPDCF324		TPDCF340				TPDCF340				TPDCF340		
		0.703**				0.264				0.201		
MCF	TPMCF324	TPMCF340a	TPMCF340c		TPMCF324	TPMCF340a	TPMCF340c		TPMCF324	TPMCF340a	TPMCF340c	
	0.054	-0.006	0.774**		-0.281	-0.325	0.859**		0.222	0,106	0.451*	
TPMCF324		TPMCF340a	TPMCF340c			TPMCF340a	TPMCF340c			TPMCF340a	TPMCF340c	
		0.939**	-0.093			0.827**	-0.539**			0,266	0,677**	
TPMCF340a			TPMCF340c				TPMCF340c				TPMCF340c	
			-0,170				-0,505*				0,762**	
FFN	TPFFN310	TPFFN326a	TPFFN326b	TPFFN326c	TPFFN310	TPFFN326a	TPFFN326b	TPFFN326c	TPFFN310	TPFFN326a	TPFFN326b	TPFFN326c
	-0.797**	0.007	0.982**	-0.752**	-0.977**	-0.781**	0.985**	-0.688**	-0.117	-0.680**	0.823**	0.924**
TPFFN310		TPFFN326a	TPFFN326b	TPFFN326c		TPFFN326a	TPFFN326b	TPFFN326c		TPFFN326a	TPFFN326b	TPFFN326c
		0.108	-0.713**	0.846**		0.793**	-0.969**	0.711**		0.382	-0.490*	0.122
TPFFN326a			TPFFN326b	TPFFN326c			TPFFN326b	TPFFN326c			TPFFN326b	TPFFN326c
			0.033	0.158			-0.767**	0.810**			-0.658**	-0.455*
TPFFN326b				TPFFN326c				TPFFN326c				TPFFN326c
				-0.628**				-0.708**				0.691**
TFM	TPTFM290	TPTFM306a	TPTFM306b	TPTFM306c	TPTFM290	TPTFM306a	TPTFM306b	TPTFM306c	TPTFM290	TPTFM306a	TPTFM306b	TPTFM306c
	-0.962**	-0.919**	-0.944**	0.988**	-0.720**	-0.742**	-0.753**	0.997**	-0.116	-	-	0.862**
TPTFM290		TPTFM306a	TPTFM306b	TPTFM306c		TPTFM306a	TPTFM306b	TPTFM306c		TPTFM306a	TPTFM306b	TPTFM306c
		0.922**	0.957**	-0.949**		0.972**	0.959**	-0.712**		-	-	0.178
TPTFM306a			TPTFM306b	TPTFM306c			TPTFM306b	TPTFM306c			TPTFM306b	TPTFM306c
			0.971**	-0.919**			0.966**	-0.739**			-	-
TPTFM306b				TPTFM306c				TPTFM306c				TPTFM306c

				-0.941**				-0.747**				-
MFN	**TPMFN270**	**TPMFN286a**	**TPMFN286b**	**TPMFN286c**	**TPMFN270**	**TPMFN286a**	**TPMFN286b**	**TPMFN286c**	**TPMFN270**	**TPMFN286a**	**TPMFN286b**	**TPMFN286c**
	-0.919**	-0.824**	-0.847**	0.925**	-0.748**	-0.767**	-0.772**	0.870**	-0.263	-	-0.641**	0.959**
TPMFN270		**TPMFN286a**	**TPMFN286b**	**TPMFN286c**		**TPMFN286a**	**TPMFN286b**	**TPMFN286c**		**TPMFN286a**	**TPMFN286b**	**TPMFN286c**
		0.859**	0.884**	-0.883**		0.948**	0.981**	-0.612**		-	0.376	-0.355
TPMFN286a			**TPMFN286b**	**TPMFN286c**			**TPMFN286b**	**TPMFN286c**			**TPMFN286b**	**TPMFN286c**
			0.904**	-0.826**			0.960**	-0.698**			-	-
TPMFN286b				**TPMFN286c**				**TPMFN286c**				**TPMFN286c**
				-0.780**				-0.677**				-0.698**

**. Correlation is significant at the 0.01 level (2-tailed).

*. Correlation is significant at the 0.05 level (2-tailed).

347

348

References

[1] S. Pérez, D. Barceló, First evidence for occurrence of hydroxylated human metabolites of diclofenac and aceclofenac in wastewater using QqLIT-MS and QqTOF-MS, Anal. Chem. 80 (2008) 8135–8145. https://doi.org/10.1021/ac801167w.

[2] V. Osorio, M. Imbert-Bouchard, B. Zonja, J.L. Abad, S. Pérez, D. Barceló, Simultaneous determination of diclofenac, its human metabolites and microbial nitration/nitrosation transformation products in wastewaters by liquid chromatography/quadrupole-linear ion trap mass spectrometry, J. Chromatogr. A. 1347 (2014) 63–71. https://doi.org/10.1016/j.chroma.2014.04.058.